TÉCNICO LISBOA

Biomass Gasification in a Drop Tube Furnace

Frederico Santos Duarte

Thesis to obtain the Master of Science Degree in

Mechanical Engineering

Supervisor: Prof. Mário Manuel Gonçalves da Costa

Examination Committee

Chairperson: Prof. Edgar Caetano Fernandes

Supervisor: Prof. Mário Manuel Gonçalves da Costa

Member of the Committee: Dr. Ana Filipa da Silva Ferreira

November 2018

“… que todo lo escrito en ellos
era irrepetible desde siempre
y para siempre,
porque las estirpes condenadas
a cien años de soledad
no tenían una segunda oportunidad sobre la tierra.”
Para ti, Mário Jorge Duarte.

Resumo

A gaseificação de biomassa é uma alternativa à utilização de recursos fósseis através da produção de gases de síntese de alta qualidade para utilização como combustível, e subprodutos sólidos. Esta tese aborda a gaseificação de biomassa num reator tubular de queda livre. Foram utilizadas partículas de palha de trigo, com dimensões entre 90 e 150 μm, tendo-se realizando um estudo da influência da temperatura do reactor tubular entre 900 e 1200 °C na produção gasosa e na formação de fuligem. A taxa de alimentação da biomassa foi de 23 g h^{-1}, e um coeficiente de excesso de ar de 0.4. Os resultados mostram que o aumento da temperatura incrementa a produção de H_2, entre ~9,5 e ~24 vol.%, CO, entre ~32 e ~34 vol.%, a razão hidrogénio/monóxido de carbono, entre 0,3 e 0,7, e a eficiência de conversão de carbono, entre ~66 e ~83%. Adicionalmente, elevadas temperaturas de funcionamento do reator tubular promovem a destruição de resíduo carbonoso, atingindo-se um valor mínimo de 133,48 mg g^{-1} biomassa seca a 1200 °C. A formação de fuligem é máxima para uma temperatura do reator tubular de 1000 °C com um valor de 3,79 mg g^{-1} biomassa seca. A temperatura de funcionamento do reator tubular tem pouca influência no poder calorifico do gás de síntese produzido. Finalmente, a eficiência energética do gás de síntese apresenta um máximo de ~49% para uma temperatura do reator tubular de 1100 °C. O estudo sugere que a temperatura de funcionamento do reator tubular óptima para o processo de gasificação é 1100 °C, a qual maximiza o poder energético do gás de síntese e a eficiência energética do processo.

Palavras-chave

Biomassa, palha de trigo, reator tubular de queda livre, fuligem, resíduo carbonoso, gás de síntese.

Abstract

Biomass gasification has the potential to replace fossil fuels through the production of a high-quality syngas to be used as fuel, and solid by-products. This thesis concentrates on the biomass gasification in a drop tube furnace. Wheat straw particles ranging from 90 to 150 μm were used as feedstock, and experiments were carried out to investigate the influence of the operating temperature of the drop tube on the gasification process between 900 and 1200 °C in the gas yield and soot formation. The biomass feeding rate was fixed at 23 g h^{-1} and air was fed to the reactor at a constant excess air ratio of 0.4. It was found that, as the drop tube temperature increased, the H_2 and CO yields, hydrogen/carbon monoxide volume ratio, and the carbon conversion efficiency increased from ~9.5 to ~24 vol.%, from ~32 to ~34 vol.%, from 0.3 to 0.7 and from ~66 to ~83%. In addition, high drop tube temperatures also have an impact on char destruction reaching a minimum of 133.48 mg g^{-1} dry biomass at 1200 °C, while soot formation reaches a maximum of 3.79 mg g^{-1} dry biomass at 1000 °C. Moreover, temperature has little influence on the heating value of the producer gas. The cold gas efficiency has a maximum at 1000 °C with a value of ~49%. The present results suggest that the optimal operating temperature of the drop tube for the gasification process is 1100 °C, which maximizes the syngas heating value and the cold gas efficiency of the process.

Keywords

Biomass gasification, wheat straw, drop tube furnace, soot, char, syngas.

Acknowledgments

First of all, I would like to express my sincere gratitude to Professor Mário Costa for accepting to be my supervisor, for guidance and exigency, for the constant follow-up and knowledge exchange, for the countless hours of meetings and innumerous e-mails, and for doing everything in his power for the project to become a reality.

To my co-worker, Salma Serghini, I would like to thank for her support through the hardest days, companionship, friendship, and work competence.

For the talks, support, lunches and ideas to improve the project throughout the year, my thanks goes to Doctor Sandrina Pereira and PhD student Ana Isabel Marques Ferreiro.

For the technical support for the experimental setup and measurements, and some patience and laughs, I would like to thank the technician Manuel Pratas and Tomás Prudente.

My mother and grand-mothers for everything they invested in my education, giving me everything I needed to succeed and for their patient dealing with me. I hope I made you proud.

To my dearest friends for making this journey meaningful not only inside the campus but mainly outside. You were my rock throughout these long five years. I am very grateful for being surrounded for you every step of the way. I hope, for the ones who already knew me and the ones who I came to know, to keep you by my side in the forthcoming challenges.

This work was supported by Fundação para a Ciência e Tecnologia through IDMEC, under LAETA, project UID/EMS/50022/2013.

Table of Contents

Nomenclature

Acronyms

CFR	Circulating flow reactor
DIA	Dynamic image analysis
DLPI	Dekati low pressure impactor
DTF	Drop tube furnace
EDS	Energy-dispersive -ray spectroscopy
EFR	Entrained flow reactor
EPA	Environmental Protection Agency
EU	European Union
FID	Flame ionization detector
GHG	Greenhouse gases
GC	Gas chromatograph
IGCC	Integrated gasification combined cycle
NDIR	Nondispersive infrared sensor
PAH	Polycyclic aromatic hydrocarbon
PCF	Pulverized coal-fired
PM	Particulate matter
RES	Renewable energy source
SEM	Scanning electron microscopy
TEM	Transmission electron microscopy
TCD	Thermal conductivity detector
TGA	Thermogravimetric analyser
WGS	Water-gas shift
WS	Wheat straw

Symbols

Roman characters

AB	Air/biomass molar ratio	(mol mol^{-1}, db)
CCE	Carbon conversion efficiency	(%)
CB	Carbon dioxide/biomass mass ratio	(kg kg^{-1}, db)
CGE	Cold gas efficiency	(%)
d_{50}	Median diameter	(µm)
d_p	Particle diameter	(m)
d_t	Thermocouple bead diameter	(m)
F_{flow}	Forced flow	(kPa)
h	Heat transfer coefficient	(W m^{-2} K)
H_2/CO	Hydrogen/carbon volume ratio	(-)
HHV	High heating value	(MJ kg^{-1})
k	Gas thermal conductivity	(W m^{-1} K^{-1})
LHV	Low heating value	(MJ kg^{-1})
M	Molecular mass	(g mol^{-1})
$\dot{m}_{air}$	Air mass flow rate	(g h^{-1})
$\dot{m}_{bio}$	Feeding mass rate of feedstock biomass	(g h^{-1})
$\dot{m}_{steam}$	Steam mass flow rate	(g h^{-1})
$\dot{m}_{N_2}$	Nitrogen mass flow rate	(g h^{-1})
$\dot{m}_{O_2}$	Oxygen mass flow rate	(g h^{-1})
NB	Nitrogen/biomass mass ratio	(kg kg^{-1}, db)
Nu	Nusselt number	(-)
OB	Oxygen/biomass mass ratio	(kg kg^{-1}, db)

Q_{syngas}	Syngas volume flow rate	($Nm^3\ h^{-1}$)
$\dot{Q_{cat}}$	Heat flow toward the thermocouple by catalyzation	(W)
$\dot{Q_{cond}}$	Heat flow toward the thermocouple by conduction	(W)
$\dot{Q_{conv}}$	Heat flow toward the thermocouple by convection	(W)
$\dot{Q_{rad}}$	Heat flow toward the thermocouple by radiation	(W)
SB	Steam/biomass molar ratio	(mol mol^{-1}, db)
SC	Steam/carbon molar ratio	(mol mol^{-1}, db)
T_g	Gas temperature	(K)
t_r	Residence time	(s)
T_r	Reactor operating wall temperature	(°C)
T_t	Thermocouple temperature	(K)
T_{steam}	Inlet steam temperature	(°C)
$\dot{V}_{air}$	Air volume flow rate	($m^3\ h^{-1}$)
$\dot{V}_{CH_4/air}$	Methane/air premixed volume flow rate	($m^3\ h^{-1}$)
$\dot{V}_{CO_2}$	Carbon dioxide volume flow rate	($m^3\ h^{-1}$)
$\dot{V}_{N_2}$	Nitrogen volume flow rate	($m^3\ h^{-1}$)
$\dot{V}_{O_2}$	Oxygen volume flow rate	($m^3\ h^{-1}$)
y_{carbon}	Carbon mass fraction from ultimate analysis	(-)
x_{O_2}	Oxygen concentration	(vol.%)
x_j	Mole fraction of products	(-)

Greek characters

ε	Emissivity	(-)
λ	Excess air coeficient	(-)
σ	Stefan-Boltzmann constant	(5.8×10^{-8} W m^{-2} K^{-4})

List of Figures

List of Tables

I. Introduction

I.1 Motivation

I.1.1 Gasification

Gasification is a thermochemical process which converts solid or liquid carbonaceous fuels into a synthesis gas or syngas that can be used to produce chemical feedstock, liquid fuels, power or gaseous fuels [1]. Figure I-1 [2] illustrates a schematic diagram of gasification, detailing the distinct syngas treatment options to produce fuel and chemicals, hydrogen, electric power and solid by-products, as well as the main options used to produce the syngas, namely, fuels (coal, petroleum char, biomass, waste, etc.) and gasifying agent (air, oxygen and steam).

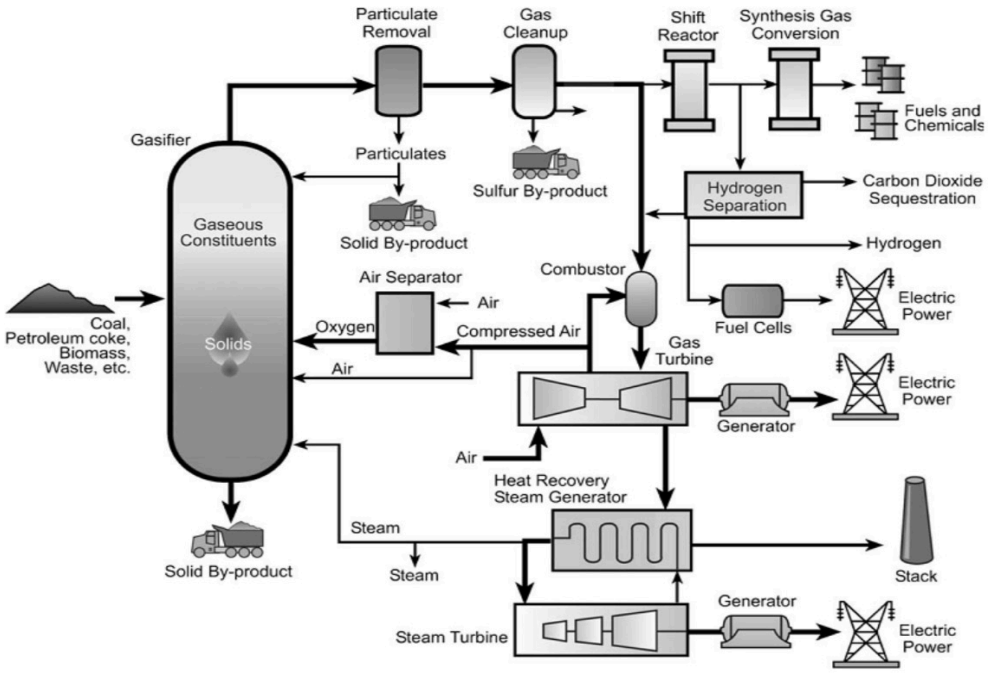

Figure I-1 - Gasification-based energy conversion options [2]**.**

Gasification has been investigated since 1659 by Thomas Shirley. Two centuries ago, coal gasification was the major responsible for lighting homes and streets, being also used for heating purposes. Years later, the focus switched to the production of synthetic fuels, used in internal combustion engines and in the replacement of fuel oil. Over the past decades, due to a variety of instabilities on the oil production and the threat of climate change, gasification reclaimed relevance [1]. Currently, as shown in Figure I-2 [3], the gasification industry is more related to the production of chemicals, liquid fuels, power and gaseous fuels. Gasification is responsible for 25% of the world's ammonia and over 30% of the world's methanol production [4], making the chemical production the largest category. At the same time, gaseous fuels are increasing their representativeness to the second largest category, mainly due

to China intervention to meet CO_2 reduction goals and to leverage in natural gas pricing. Figure I-3 [3] illustrates the worldwide gasification capacity from the 1970s to future expectations by 2021, showing an increased demand for syngas.

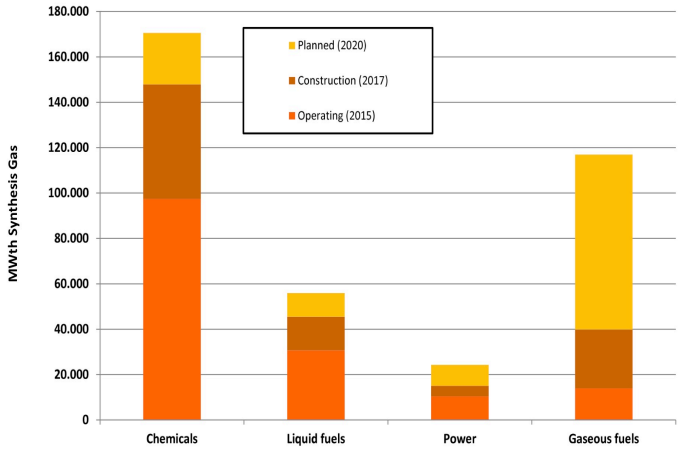

Figure I-2 - End use application of syngas [3].

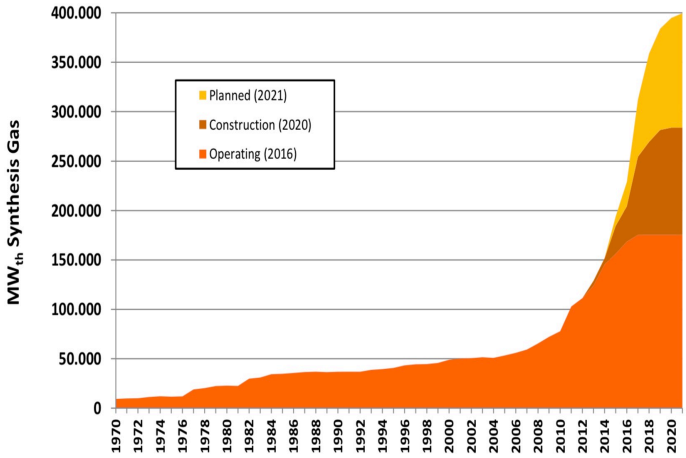

Figure I-3 – World cumulative gasification capacity [3].

The gasification process can be performed in different atmospheres, such as oxygen, air, carbon dioxide, steam or blends, and high temperature and pressure, originating the formation of desired components, such as H_2 and CO, and undesired components, such as soot, char, tar, carbonaceous gases, NO_x and SO_x. Table I-1 [5] shows the comparison of emissions between pulverized coal fired (PCF) and integrated gasification combined cycle (IGCC) power plants. It can be verified that the emissions of CO_2, SO_2, NO_x and PM_{10} are lower for IGCC plants, with a main distinction for SO_2, NO_x and PM_{10}. The PM is a variety of solid, liquid or both particles suspended in the atmosphere. In particular PM_{10} stands for particles with an aerodynamic diameter of 10 μm or less. Considering the

small size (< 2.5 μm), PMs have large residence time, ranging long distances in the atmosphere becoming a global problem.

Table I-1 - Comparison of emissions between PFC and IGCC power plants [5].

Emission	PCF Plant	IGCC Plant
CO_2 (kg/MWh)	0.770	0.680
SO_2 (kg/MWh)	0.680	0.045
NO_x (kg/MWh)	0.610	0.090
PM10 (kg/10 MWh)	0.450	0.110

Nowadays, biomass became the fourth largest final energy consumption, accounting for 14% of the world's energy consumption with practically 2.6 billion people relying on biomass for energy, as illustrated in Figure I-4 [6]. As biomass is considered a CO_2 neutral fuel source, these numbers tend to grow, as EU set for 2030 to reduce its GHG emissions by 40% relative to the emissions from 1990 [7]. The CO_2 neutrality of biomass relies on the equilibrium between the CO_2 released to the atmosphere to generate heat and power through combustion, and the CO_2 absorbed by the biomass from the atmosphere through its photosynthesis in the growing stage. Therefore, the net addition of CO_2 to the atmosphere is considered to be zero.

Biomass gasification provides a mitigation on the dependence of carbon-rich fossil fuels in the production of power, fuels and chemicals, and, at the same time, a reduction on the emissions of GHG, meeting the continuously development of policies and regulations imposed by national governments. Therefore, the understating of biomass gasification at a laboratory scale is a preliminary step in evaluating its relevance for industrial applications.

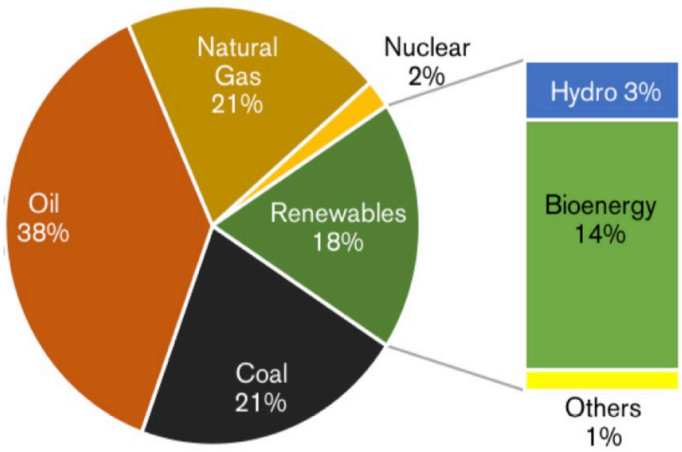

Figure I-4 - World's gross final energy consumption in 2013 [6].

Besides the formation of the syngas, solid particles, formed mainly by carbon, are produced in the gasification process. These particles come from different formation processes and are known as soot an char. Char is formed in the thermal breaking of the biomass, presenting larger particles (~ 100 μm), and soot has a more complex formation process, therefore it needs to be studied. In Section I.1.2 a comprehensive resume of the soot formation is presented.

I.1.2 Soot

Soot is the term given for small spherical particles constituted mainly of carbon (for instance, C_4H_2 and C_8H_2), formed during the combustion of carbonaceous fuels under sub-stoichiometric conditions and high temperatures [8]. Furthermore, the soot particles are the result of the agglomeration of many spherical carbon and inorganic particles up to a size of 200 nm. Figure I-5 [9,10] illustrates a transmission electron microscopy (TEM) and a scanning electron microscopy (SEM) image of soot particles.

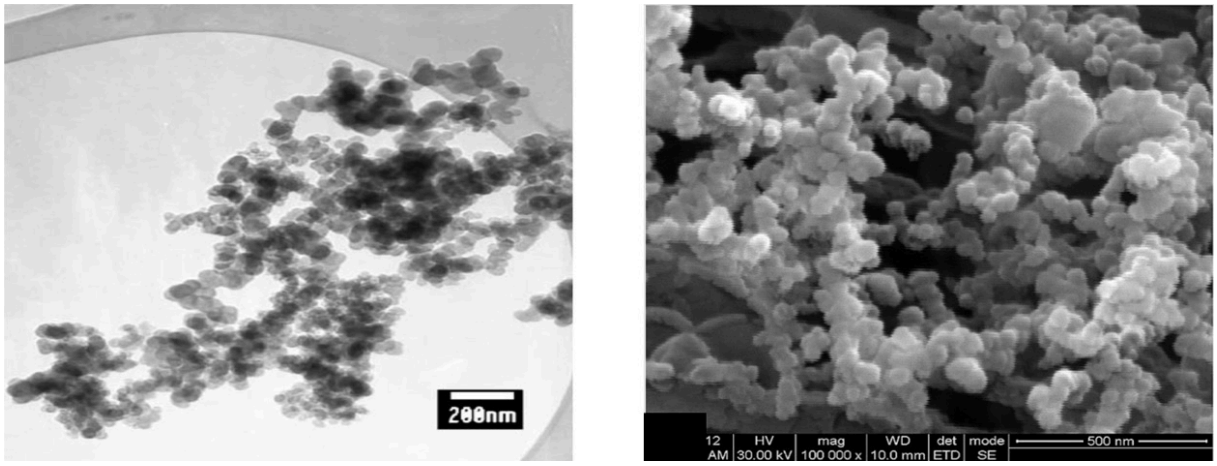

Figure I-5 - TEM (left) and SEM (right) images of aggregated soot particles [9,10]**.**

Several studies reported the soot damaging effects at different levels. *Bond et al.* [11] studied the impact of soot on the climate system and concluded that soot particles represent approximately two thirds of the carbon dioxide impact and have larger impact than methane, due to the capacity of the soot particles to absorb radiation, which heat the atmosphere, and when released to the air promotes the greenhouse effect. *Agarwal et al.* [12] reported that soot particles exhibits threatening repercussions on the human and animal health, as a result of its small size. The PMs infiltrate the respiratory and cardiovascular systems, leading to lung malfunction and premature death. The smaller PM is, the deeper it penetrates the respiratory system, as illustrated in Figure I-6 [13]. Also, soot contribute for serious problems in the industry, namely, the formation of dark exhaust plumes, the agglomeration of soot on the walls, the reduction of the carbon conversion efficiency (CCE), since soot particles are carbon without adding value, and can affect the turbine durability and integrity, lowering the turbine performance [14,15].

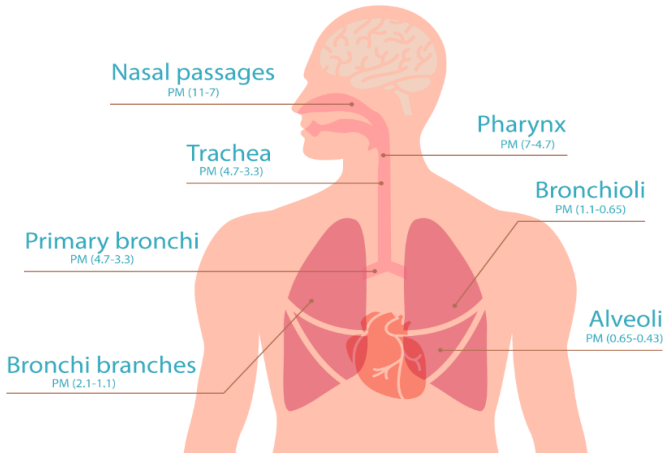

Figure I-6 - Deposition of PMs on the respiratory system according to its size in µm [13].

The Environmental Protection Agency (EPA) aims to reduce actual soot emissions to 12 µg m^{-3} by 2020, according to The Clean Air Pact [16]. In order to achieve this goal and to reduce the remaining damaging effects, activities in the research field of soot formation on combustion, pyrolysis and gasification of carbonaceous fuels became more active. Thus, understanding the characteristics and the conditions of soot formation in biomass gasification is essential to improve the efficiency of biomass gasification and to reduce the high costs of cleaning the final syngas.

I.2 Literature Review

I.2.1 Gasification Theory

Gasification is a thermochemical process whereby a solid or liquid carbonaceous fuel is converted into a gaseous fuel, known as synthesis gas or syngas, using a controlled amount of a gasifying agent at elevated temperatures [17,18]. Heterogeneous and homogeneous reactions occur in the gasification process, for example, solid carbon with oxygen, water vapor or carbon dioxide, oxygen with hydrogen and carbon monoxide, and carbon monoxide with water vapor, among others [1]. Depending on the fuel, the gasifier type and the operating conditions, the gasification thermochemical process outputs differ, namely, gas composition, ash, soot and tar. In order to assess the quality of the syngas production, parameters, such as the low heating value (LHV), carbon conversion efficiency (CCE), cold gas efficiency (CGE) and hydrogen/carbon monoxide ratio (H_2/CO) must be accounted.

I.2.1.1 Stages of Gasification

Biomass gasification occurs through different and complex steps, often overlapping, making harder to outline a clean path of the process. Sainsaniwal *et al.* [19], proposed the following sequence of thermochemical reactions:

- Drying;
- Pyrolysis;
- Oxidation;
- Reduction.

Table I-2 [1] reveals the most important thermochemical reactions in the gasification process and the heat of reactions for a temperature of 25 °C.

Table I-2 - Main gasification reactions [1]**.**

Reaction Type	Reaction
R_1 (*Boudouard*)	$C + CO_2 \leftrightarrow 2CO + 172\ kJ/mol$ [20]
R_2 (*Water-Gas* or *steam*)	$C + H_2O \leftrightarrow CO + H_2 + 131\ kJ/mol$ [21]
R_3 (Hydrogasification)	$C + 2H_2 \leftrightarrow CH_4 - 74.80\ kJ/mol$ [21]
R_4	$C + 0.5O_2 \leftrightarrow CO - 111\ kJ/mol$ [20]
R_5	$C + O_2 \leftrightarrow CO_2 - 394\ kJ/mol$ [21]
R_6	$CO + 0.5O_2 \leftrightarrow CO_2 - 284\ kJ/mol$ [22]
R_7	$CH_4 + 20_2 \leftrightarrow C0_2 + 2H_2O - 803\ kJ/mol$ [20]
R_8	$H_2 + 0.5O_2 \leftrightarrow H_20 - 242\ kJ/mol$ [22]
R_9 (*Water Gas Shift reaction*)	$CO + H_20 \leftrightarrow CO_2 + H_2 - 41.2\ kJ/mol$ [22]
R_{10}	$2CO + 2H_2 \leftrightarrow CH_4 + C0_2 - 247\ kJ/mol$ [22]
R_{11} (*Methanation*)	$CO + 3H_2 \leftrightarrow CH_4 + H_2O - 206\ kJ/mol$ [22]
R_{12}	$CO_2 + 4H_2 \leftrightarrow CH_4 + 2H_2O - 165\ kJ/mol$ [21]
R_{13} (*Methane Steam Reforming*)	$CH_4 + H_2O \leftrightarrow CO + 3H_2 + 206\ kJ/mol$ [20]
R_{14}	$CH_4 + 0.5O_2 \leftrightarrow CO + 2H_2 + 36\ kJ/mol$ [20]

Drying

Biomass moisture is of utmost importance in the gasification process, interfering in the quality of the producer gases. Biomass feedstock can have a moisture content up to 60% [23], but the optimization of gasification systems is reached for biomass moisture content between 10% and 20% [24,25]. Low content of moisture reduces the extra energy needed to vaporize the excess of water; when moisture content is high there is the need to pre-dry the raw biomass in order to increase the process efficiency.

As the biomass enters the gasifier, the release of water starts at around 100 °C, as shown by Equation $(\mathrm{I}-1)$:

$$Moist\ feedstock + Heat \rightarrow Dry\ feedstock + H_2O \qquad (\mathrm{I}-1)$$

Drying is assumed to be the only step at low temperature.

Pyrolysis

The pyrolysis process occurs between 125 and 500 °C, and consists on the biomass thermal breakdown, in the absence of air or oxygen, into relatively smaller and simpler molecules (condensable and noncondensable) of char and volatiles, as represented by Equation $(\mathrm{I}-2)$:

$$Dry\ feedstock + Heat \rightarrow Volatiles + Char \qquad (\mathrm{I}-2)$$

Pyrolysis is performed in two different stages. The first stage consists on the loss of hemicellulose, cellulose and part of lignin, occurring at temperatures between 125 to 500 °C. Then, the second stage reflects the loss of residual lignin at temperatures above 500 °C [26]. Chemical reactions taking place under 300 °C are exothermic, while reactions above 300 °C are endothermic [19].

Depending on the biomass properties and pyrolysis conditions, different products can be obtained [27]. Char is composed manly by carbon and, in lower quantities by ash, oxygen and hydrogen. Volatiles can include H_2, CO, CO_2, H_2O, CH_4, NH_3, several hydrocarbons and tar, which when subject to secondary reactions may produce soot.

Figure I-7 [13] shows the soot process formation [28]. Tar is the primary responsible of soot formation. The tar obtained in pyrolysis is mainly formed by PAHs. At high temperatures the PAHs suffer cracking, Equation $(\mathrm{I}-3)$, and reforming processes, Equation $(\mathrm{I}-4)$ and Equation $(\mathrm{I}-5)$:

$$TAR \longrightarrow CO + CO_2 + CH_4 + H_2 + soot \qquad (\mathrm{I}-3)$$

$$TAR + H_2O \longrightarrow H_2 + CO \qquad (\mathrm{I}-4)$$

$$TAR + CO_2 \longrightarrow H_2 + CO \qquad (\mathrm{I}-5)$$

Ma [29] proposed that the soot formation mechanism is dominated by the cracking of different hydrocarbons and hetero-aromatic compounds consisting of O, S, and N. Soot is mainly formed by carbon (> 90 wt.%) and some ash [28]. The most accepted theory of the mechanism of soot formation is divided in four stages: nucleation of soot particle, particle coagulation, particle surface reactions and particle agglomeration [30].

Drying and pyrolysis may take place simultaneously and complete instantaneously due to the reactor high heating rates.

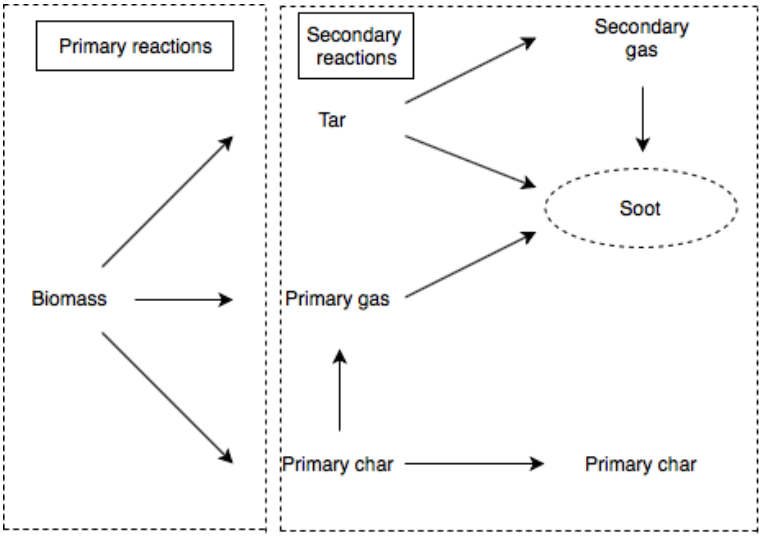

Figure I-7 – Soot process formation [28].

Oxidation

The oxidation process occurs under exothermic chemical reactions between pyrolysis products and oxygen, being the oxygen controlled by excess air coefficient (λ). Gasification can be acknowledge as a fuel-rich combustion in a controlled environment, with typical values of λ ranging between 0.20 and 0.50 [31]. Under similar conditions, oxidation reactions are faster than gasification reactions [32], providing the heat required to promote the endothermic gasification reactions.

This stage is crucial for the gasification process. Besides creating heat, oxidation converts the pyrolysis products on the desired gases, such as CO and H_2. Thus, parameters, such as temperature, pressure and the gasifying agent play a major role on the quality of the produced gas [19,33].

To better understanding of the oxidation process, Table I-2 [1] lists the main exothermic reactions: R_4, R_5, R_6, and R_8. Reaction R_4 is the partial oxidation reaction and R_5 is the complete oxidation reaction, producing carbon monoxide and carbon dioxide, respectively, from solid carbonized fuel (i.e. char and soot) and oxygen. The remaining reactions consist in the combination of gases, such as carbon monoxide, hydrogen and methane with oxygen, to produce carbon dioxide and water vapors, respectively.

Reduction

Heterogeneous gasification reduction reactions occur between pyrolysis products, being the most important the char gasification reactions. In these reactions, char reacts with different gasifying media, such as carbon dioxide, hydrogen, steam and methane. Blasi *et al.* [27] studied the rate of gasification,

and proposed char gasification as the rate controlling step. Furthermore, hydrogen reactions were observed to be the slowest, followed by carbon dioxide reactions and steam reactions.

Reduction reactions take place under high temperatures and reducing atmospheres, converting sensible heat of the gases and char into chemical energy in the producer gas [19].

As shown in Table I-2 [1], the reduction process can be described by endothermic chemical reactions R_1 and R_2, and exothermic chemical reactions R_3, R_9, R_{10}, R_{11} and R_{13} [20]. During these reactions carbon dioxide and water vapor are reduced into combustible products, such as carbon monoxide, hydrogen and methane.

Reaction R_1 is the *Boudouard reaction*, and reaction R_2 is the *water-gas reaction*, both reduce char into combustible products reacting with carbon dioxide and steam, respectively. Reaction R_9 is the *Water Gas Shift (WGS) reaction*, which is extremely relevant to control the H_2/CO ratio, due to the consumption of carbon monoxide and steam to produce hydrogen and carbon dioxide. And finally, if methane is the desired product, the *hydrogasification reaction* (R_3) and the *methanation reactions* (R_{10}, R_{11} and R_{13}) are the important chemical reactions because methane is formed at the expense of char, and carbon monoxide with hydrogen, respectively. In these equations, high temperatures may reverse the reaction direction.

I.2.1.2 Gasification Reactors

Experimental studies on gasification are, usually, carried out in three different reactor configurations according to the way that biomass interact with oxygen steam or carbon dioxide, namely, moving bed, fluidized bed and entrained flow reactors [1,34]. Depending on the interaction, the temperature on the gasifier differs. Figure I-8 [3] shows the temperature profiles along the gasifiers height, and schematically represents the gasifiers types regarding fuel feeding and gasifying agent inserting zones, and the main output zones, such as product gases and ashes. Their main characteristics are summarized in Table I-3 [1,31] and Table I-4 [38–53], which compare the main characteristics of moving bed and fluidized bed gasifiers, and entrained flow gasifiers and drop tube furnaces, respectively.

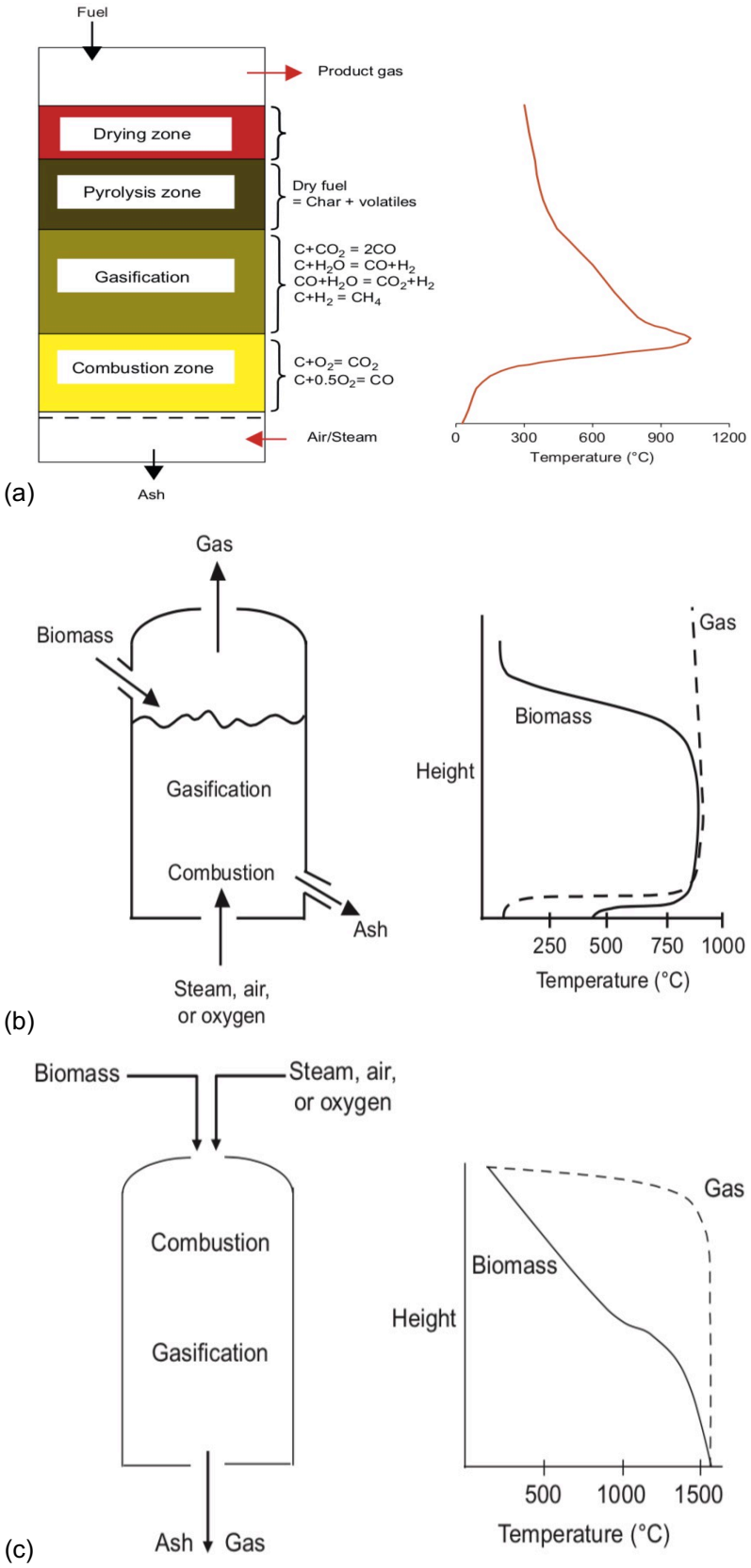

Figure I-8 - Gasifier types and the respective temperature profile. (a) Updraft gasifier, (b) bubbling fluidized bed gasifier, and (c) top fed entrained flow gasifier [3].

Table I-3 – Main characteristics of moving and fluidized bed reactors [1,31].

Characteristic	Equipment	
	Moving Bed	**Fluidized Bed**
Particle size (mm)	< 51	< 6
Maximum temperature (°C)	Up to 1090	Up to 1000
Application	Small capacities	Intermediate units
Tar (g Nm^{-3})	0.10 – 100	1 – 50
Gas LHV (MJ Nm^{-3})	4 – 6	3.30 – 5.30
Soot (g Nm^{-3})	0.10 – 10	2 – 20

Table I-4 - Main characteristics of DTFs and EFRs [38–53].

Characteristic	Equipment	
	Drop Tube Reactor	**Entrained Flow Reactor**
Dominant heat transfer mechanism	Radiation	Convection
Particle size (mm)	< 1	< 1
Maximum temperature (°C)	Up to 1500	Up to 2000
Maximum heating rate (°C s^{-1})	~ 10^3 to 10^4	~ 10^4 to 10^5
Residence time (s)	0.30 – 14	0.40 – 8
CCE (%)	55 – 90	50 – 95
Gas LHV (MJ kg^{-1}, db)	3 – 10	7 – 9
Soot (g kg^{-1}, db)	1 – 60	1 – 50

Moving bed reactor and fluidized bed reactor

The moving bed gasifier is the most economical and simpler configuration, consisting in a fuel bed being held stationary or moving, while the chemical reactions occur. In an updraft moving bed (Figure I-8 (a) [3]), the fuel particles enter at the top and move downward though the stages of gasification, leaving the product from the top as well. The gasifying agent enters at the bottom, reacting with hot ash and unconverted chars, exceeding the ignition temperature producing a peak [1]. The products leave from the boiler top. Besides the updraft gasifier, the moving bed gasifiers can have two more configurations: downdraft and crossdraft [35]. The moving bed is not very effective mixing and transferring heat, which creates problems across the cross-section of the gasifier, such as nonuniform distribution of fuel, temperature and gas composition. Frequently, moving bed gasifiers use large fuel particles to ensure a better bed permeability and efficient heat and mass transfer. Depending on the gasifier, tar and particulate matter production can achieve low values (the updraft gasifier presents the worst results), requiring relatively simple gas-cleaning systems. The product gases presents a small

and good range of values of volume and energy content (the updraft gasifier present the best results) [1,31].

Contrary to the moving bed gasifier, in the fluidized bed gasifier the gasifying agent conveys the fuel particles across the reactor. It is notorious the higher capacity of mixing and heat transfer, which results from a mixing between the gasifying agent and inert solids (bed materials), such as sand or alumina [33]. The bubbling fluidized bed gasifier, (Figure I-8 (b) [3]), consists in feeding the fuel particles through the top of the gasifier and the gasifier agent through the bottom, both at relatively high velocities. The bed materials enter in contact with the fuel, rapidly increases the temperature to achieve a uniform value, and causes rapid drying and pyrolysis. As the gasifying agent rises, reacts to produce the final gas, leaving at the top of the gasifier. Two types of fluidize bed gasifier are presented in the literature: bubbling and circulating [19,26,33]. In fluidized bed gasifier, the gasification process have a better development with small fuel particles [33], tar and particulate matter formation have higher values due to higher temperatures, typical values are ~10 g Nm^{-3} [36] and from 2 – 20 g Nm^{-3} [31], respectively. The broad application of this gasifier is in intermediate units, with limitations in carbon conversion.

Warnecke [37] studied the differences between moving bed and fluidized bed gasifiers, looking to the bed material, use of energy, and environmental and economic impact, concluding that no significant differences exist between them.

Entrained flow reactor

The entrained flow reactor (EFR) is a popular technology for large scale gasification of coal and petroleum cokes. In Figure I-8 (c) [3] is presented a top fed entrained flow reactor where the fuel particles and the gasification agent are introduced at the top of the gasifier, and the product gas along with molten slag, exits at the bottom of the reactor. The main advantage of this technology is that the fuel particles are subject to high temperature and pressure during a short residence time, which results in gasification reactions taking place at elevated heating rates. These operating conditions result in low tar production, high carbon conversion, and a possible low methane content and high efficiency for the production of syngas [38–53]. Furthermore, the suitability of the entrained flow reactor is controversial for biomass application considering the low residence time (the particles must be very fine) and the alkali content (promotes the formation of corrosive ash) [20,54,55]. Entrained flow reactors can be divided into two types: top-fed downflow and the side-fed upflow [1].

In order to support the industry of commercial biomass gasification is of utmost importance to have simple and rapid tools able to predict the performance indicators in order to access the influence of the biomass characteristics and operating conditions on gasification. For these reasons, the drop tube reactor was developed at a laboratory scale. The drop tube reactor (DTF) can provide extremely useful information, but the mechanism governing the heat transfer is radiation instead of convection in a typical entrained flow reactor. Thus, the temperatures and the heating rates in the drop tube reactors are lower than in entrained flow reactors, as shown in Table I-4 [38–53].

I.2.1.3 Performance Parameters

Many performance indicators enable to evaluate the efficiency of the gasification process to assess the quality of the producer gas. According to *Villeta* et. al [31], the main parameters are as follows.

The low heating value (LHV) is the amount of heat produced by a complete combustion of the syngas. It takes into account the chemical composition of the syngas and its respective heating value.

The carbon conversion efficiency (CCE) is the "rate between the carbon leaving the gasifier in the syngas (as CO, CO_2, etc.) and the carbon entering the system":

$$CCE = \frac{Q_{syngas} \sum_i^n x_{carbon,i}}{\dot{m_{bio}} y_{carbon}} \quad (\mathrm{I}-6)$$

The cold gas efficiency (CGE) is defined as "the ratio between the chemical energy leaving the system associated with the cold and tar-free syngas and the chemical energy entering the system associated with the biomass":

$$CGE = \frac{Q_{syngas} LHV_{syngas}}{\dot{m_{biom}} LHV_{bio}} \quad (\mathrm{I}-7)$$

Finally, the hydrogen/carbon monoxide (H_2/CO) volume ratio in the producer gas is another performance indicator.

I.2.2 Effect of the Operating Parameters

In this section, a literature review is made concerning the operating conditions of the ERFs and DTFs, and their impact on the composition, quality and final applications of the produced gas. The review focus on fuel particles physical and chemical properties, namely, sizes and chemical composition, and gasifier operating conditions, such as operating temperature, gasifying agent, residence time, among others. Table I-5 shows a summary of the experimental studies on biomass gasification in EFRs and DTFs, including fuels and sizes, materials and methods, experimental conditions and the main results of each study. Numerous types of fuels are listed, from woody and non-woody biomass to lignite.

Table I-5 – Most relevant work on biomass gasification on DTFs and EFRs.

Reference	Fuels	Methods	Conditions	Main results
Hernández et al. [38] Influence of relative biomass/air ratio, temperature and steam content of the gasifying agent, on the properties of char produced.	Dealcoholised marc of grape < 500 μm	DTF μ-GC TGA SEM FTIR	T_r: 750 – 1200 $\dot{m}_{bio}$= 620 – 1830 $\dot{m}_{H_2O}$: 0 – 1600 $\dot{m}_{O_2}$: 0 – 2400	There's a trade-off between fuel conversion and char specific surface area, discouraging its application as activated carbon. Higher temperatures have positive effects on gasification process regardless the gasifying agent used.
Billaud et al. [39] Influence of addition of steam, carbon dioxide and oxygen are investigated for different temperatures and operating conditions.	Beech wood 315 – 450 μm	DTF μ-GC, TCD TGA	T_r: 800 – 1400 λ: 0.24 – 0.61 t_r= 4.30 $\dot{m}_{CO_2}$= 0.4 $\dot{m}_{H_2O}$= 0.62 $\dot{m}_{N_2}$= 1.5 $\dot{m}_{O_2}$: 1-2.50	Addition of H_2O or CO_2 influenced carbon distribution at 1200 and 1400 ºC, decreasing the amount of carbon on tar and soot. Oxidant presence on the atmosphere increased char conversion, decreasing the soot formation. CCE increased with λ up to 1200 ºC, starting to decrease at higher temperatures. Increased λ decreased the tar yield.
Umeki et al. [40] Investigation on tar and soot formation impregnating biomass with alkali metal species.	Raw and potassium-impregnated pine sawdust 90 – 200 μm	DTF μ-GC SEM	T_r: 900 – 1400 t_r: 10.3 – 14.7 $\dot{m}_{bio}$= 4.8 $\dot{V}_{N_2}$= 0.18 $\dot{V}_{CO_2}$= 0.26 (representing 5.1 vol.%, the rest is N_2)	Impregnated biomass reduced tar and soot formation up to 1100 °C. Catalytic activities occurred in both sold and gas phases during devolatilization and secondary decomposition.

Reference	Fuels	Methods	Conditions	Main results
Hernández et al. [41] Effect of the addition of steam to air as gasifying agent and temperature.	Dealcoholised marc of grape < 500 μm	EFR GC-TCD	T_r: 750 – 1150 T_{steam} = 250 *SB*: 0 – 3.19 *AB*: 0 – 2.62 $\dot{V}_{air}$: 0 – 3 $\dot{m}_{bio}$: 580 – 2230 $\dot{m}_{steam}$: 0 – 1500	Increased steam content improves the quality of the gas, promoted char and tar steam reformation, and WGS reactions. Optimal steam-air mixture is between 40 – 70 mol.% steam. Higher temperature increased CO and H_2 gas products for air, and H_2 and CH_4 for steam.
Schneider et al. [42] Influence of particle size, type of fuel, temperature and gasifying agent to evaluate the decentral use of biomass on a small-scale EFR.	Beech wood 40 – 110 μm Beech and spruce 200 – 250 μm 250 – 500 μm 500 – 1000 μm	EFR GC	T_r: 950 – 1100 λ: 0.31 – 0.43 t_r: 6 – 8 $\dot{m}_{bio}$: 1000 – 2000 $\dot{V}_{air}$ = $\dot{V}_{CO_2}$ = $\dot{V}_{O_2}$: 2 - 4 $\dot{V}_{N_2}$ = 2	Maximum carbon conversion, cold gas efficiency and specific syngas volume, is achieved with smaller particles, at 1100 °C, obtaining H_2/CO ratio of 0.75. High nitrogen dilutions of the product gas and small residence times is one of the main problems, since it's used N_2 and air with the fuel feeding.
Qin et al. [43] Influence of reaction temperature, steam/carbon molar ratio, excess air ratio and biomass type, on the solid, liquid and gas products.	Wood 280 μm Straw 170 μm	DTF NDIR CG-TCD	T_r: 1000 – 1350 *SC*: 0, 0.5 and 1 λ: 0.25, 0.35 and 0.5 t_r: 2 – 3 x_{O_2}: 5 – 10 $\dot{V}_{air}$: 10 – 19 $\dot{m}_{bio}$: 546 – 570 $\dot{m}_{steam}$: 0, 198 and 402 $\dot{V}_{N_2}$: 21 – 30	At the highest temperatures no tar and some soot particles were contained in the syngas. Higher temperatures increased the yield of produced gases and soot but eliminated the production of tar. Steam presence increased produced gases, but decreased CO yield, and reduced the soot formation. Air excess decreased increasing the CO_2 yield and reducing the soot formation.

Reference	Fuels	Methods	Conditions	Main results
Zhang et al. [44] Influence of nitrogen, steam, and oxygen, at different range temperatures, on tar destruction and soot formation.	Hinoky cypress sawdust < 100 μm	DTF μ-GC TGA	T_r: 600 – 1400 *SB*: 0.7, 1.4 and 2.3 *OB*: 0.34 and 0.6 t_r: 2 – 4 $\dot{m}_{bio}$: 60 – 70	Tar evolution decreased with temperature; complete destruction was achieved at 1200 °C. Soot formation reached its peak at 1100 °C; Steam and partial oxidation decreased soot formation. Soot formation increased due to decomposition of hydrocarbon gases at 800 °C; at 1100 °C the process reverts due to formation of CO and H_2.
Yu et al. [46] Influence of OC, λ and reactor temperature, on the produced gas composition, gasification index and tar yield.	Rice straw < 300 μm	EFR GC	T_r: 800 – 1200 λ: 0.15 – 0.35 t_r: 1.9 – 5.5 $\dot{V}_{N_2}$: 1 – 1.8 $\dot{m}_{bio}$= 360	O_2-enriched gasification raised the LHV, the produced gas yield, CCE, H_2/CO, and decreased the yield of tar. Higher λ decreased H_2, CO, LHV and the tar yield, and increased the produced gas yield and CEE. Temperature rise increased H_2 and CO yields, LHV, produced gas yield and CEE and decreased CO_2 yield.
Lapuerta et al. [47] Potential of using the same equipment for different types of biomass, through the influence of biomass/air ratio and reaction temperature.	Pinus pinaster Grapevine and olive Sawdust Marc of grape < 800 μm	DTF TGA GC	T_r: 750 – 1350 *AB*: 0.5 – 3 t_r: 0.38 – 1.49 $\dot{V}_{air}$: 0 – 3 $\dot{m}_{bio}$: 650 – 3000 $\dot{m}_{O_2}$: 1790 – 7370	Agricultural wastes are slightly more efficient for gasification than forestry and industrial. Lower *AB* increased the gas yield production and concentration. Carbon conversion was kept constant through different temperatures. Higher temperatures produced H_2-rich gas.

Reference	Fuels	Methods	Conditions	Main results
Zhou et al. [48] Influence of biomass-oxygen ratio, residence time and temperature, on gasification in a bench scale EFR.	Rice husk Sawdust Camphor wood 149 – 250 µm	EFR GC	T_r: 1000 – 1400 T_{O_2}= 400 *OB*: 0 – 1.4 t_r: 0.4 – 2 $\dot{m}_{bio}$: 60– 120 $\dot{V}_{N_2}$: 3 – 10	Temperature increased H_2 and CO production, and cold gas efficiency. Shorter residence time resulted in incomplete gasification and a longer time lead to an unsteady feeding and reduced efficiency. More O_2 strengthen the gasification and improved CCE, but reduced LHV and H_2/CO ratio.
Qin et al. [49] Insight into the effects of types of biomass, residence time, feeder air flow, oxygen concentration, excess air ratio, steam/carbon ratio, and rector temperature.	Wood 310 µm Straw 130 µm Dried lignin 280 µm	EFR NDIR µ-GC TGA	T_r: 1000 – 1400 *SC*: 0, 0.5 and 1 λ= 0.3 t_r: 2.5 – 2.7 x_{O_2}: 5 and 21 $\dot{V}_{air}$: 6 – 14 and 2.1 – 10.2 $\dot{m}_{bio}$: 384 – 954 $\dot{m}_{steam}$: 0 – 31074 $\dot{V}_{N_2}$: 6 – 14 and 2.1 – 10.2	Adding steam lowered char and soot yield, and increased the total dry gas yield. Longer residence time and larger feed air flow reduced soot yield and kept constant H_2 and CO yields. High temperatures and steam addition, with oxygen, reduced soot yield, and increased H_2 and CO yield. Biomass with high potassium content presented much lower soot yield.
Hernández et al. [50] Influence of biomass particle size and residence time on the gasifier performance and produced gas quality.	Dealcoholised marc of grape < 500 µm	DTF µ-GC	T_r: 750 –1150 t_r: 1.36 – 1.92 $\dot{m}_{bio}$: 580 - 1710 $\dot{m}_{air}$: 1700 - 2400	A particle size reduction and longer residence time improved the overall gas quality, LHV, CGE, H_2/CO ratio and CCE. The best results were obtained for a particle size of 0.5 mm. Smaller particles released more volatiles during pyrolysis.

Reference	Fuels	Methods	Conditions	Main results
Goktepe et al. [51] Influence of flow manipulation by adding synthetic jet in feeding line affects dispersion of fuel particles and soot formation.	Pine sawdust 63-125 µm	EFR µ-GC Laser extinction	$\dot{V}_{air}$: 0.14 λ= 0.8 F_{flow}: 0 – 1.11	Vortex rings decreased soot formation, dispersing fuel particles and mixing gas. Higher gas temperatures due to vortex rings didn't affect the soot formation. At 60 mm downstream of the burner soot exhibits its maximum formation; the addition of the synthetic jet reduced this value.
Goktepe et al. [52] Investigation on soot reduction method by forcing dispersion of biomass particles.	Pine sawdust 63-125 µm	Flat flame burner DTF DIA 3 CCD camera	$\dot{m}_{bio}$: 10.7 – 15.9 $\dot{V}_{N_2}/\dot{V}_{CH_4/air}$: 1 – 3	Soot had a peak at a distance of 22 mm from the burner outlet. Soot increased with the decreasing inter-particle distance.
Septien et al. [53] Influence of steam, particle size and temperature, on gasification.	Beech sawdust 313 – 400 µm 730 – 900 µm	DTF µ-GC FTIR	T_r: 1000 – 1400 T_{steam} = 180 t_r: 2.2 and 4.4 $\dot{m}_{bio}$: 18 – 78 $\dot{m}_{steam}$: 12.1 – 15.9	Adding steam to the atmosphere at 1200 and 1400 °C lowered char and soot yield, and increased the total dry gas yield, due to steam gasification of solids (char and soot), and steam reforming and WGS. At 1400 °C, char seemed to be completely gasified and soot yield represents 5 wt.% of initial dry biomass.

Based on the comprehensive summary presented in Table I-5, several conclusions can be attained. Different parameters can modify the gasification output. In instance for the producer gas, the increase in the H_2 yield can be promoted by higher operating temperatures [38,42,44,46,47,49,50] or the addition of H_2O [41,49] or CO_2 [39] as gasifying agent. But it decreases with the addition of oxygen as gasifying agent [43,46,47,49], higher residence time [48] or higher particle diameter [50]. On the other hand, for the solid particle formation, the soot formation is promoted with higher operating temperatures [44,49]. Although, other parameters can decrease it production, specifically, the addition of oxygen, H_2O [44] or CO_2 [39] as gasifying agent, the impregnation of biomass with alkali elements [40] or the use of alternative methods, consisting in the addition of a synthetic jet or he change of the fuel dispersion [51,52].

This work will provide a clear distinction between the particulate matter (PM) collected in the solid sampling unit and the formation of soot and char, as its discussed during Chapter III. Since the literature did not provide an evident way to separate soot from char formation.

In the following paragraphs its discussed thoroughly the main parameters governing our gasification system, namely, the operating temperature, air as gasifying agent, residence time and particle diameter.

I.2.2.1 Effect of the Operating Temperature

On biomass gasification process, the reactor temperature is one of the operating conditions with more influence on the producer gas composition and properties. Figure I-9 [38,42,44,46,47,49,50] shows results obtained by *Hernández et al.* [38,50], *Schneider et al.* [42], *Zhang et al.* [44], *Yu et al.* [46], *Lapuerta et al.* [47] and *Qin et al.* [49], which analysed the influence of the temperature on the biomass gasification process, namely on the production of H_2, CO, soot and carbon conversion. The experimental tests were carried out with different values of excess of air, different biomass and different size ranges.

In general, the production of H_2 and CO increased with the increase of the temperature. At higher temperatures, the reforming reaction of CO_2 with char (*Boudouard*, Table I-2 [1]) and tar (Equation $(\mathrm{I}-5)$) increases, promoting the formation of H_2 and CO, while the consumption of CO_2 increases. For temperatures above 1200 °C, the *WGS reaction* (R_9, Table I-2 [1]) is reversed, promoting the consumption of CO_2. And, in the temperature range of 700 to 900 °C, the steady production of CO may be related to the *WGS reaction* (R_9, Table I-2 [1]) acceleration due to the high heating rates. The soot formation in the gasification process starts at 900 °C, exhibiting a maximum formation between 1100 and 1250 °C, and decreasing for higher temperatures. These results are in agreement with the carbon conversion results. In general, the carbon conversion augmented with the increase of the temperature. Results from *Zhang et al.* [44] and *Schneider et al.* [42] reveal how the stages of gasification influence the carbon conversion. From temperatures under 900 °C [44] and 1000 °C [42], the carbon conversion increases due to the gasification reactivity of the volatiles, char and soot. For temperatures from 900 to 1100 °C [44], and from 1000 to 1050 °C, a weighted distribution occurs between the decomposition of hydrocarbon gases (Equation $(\mathrm{I}-2)$) and the carbon gasification

reactions, promoting the formation of soot in this temperature range. For the remaining temperatures, the increase on the carbon conversion is due to the consumption of soot and CO_2, promoting the formation of H_2 and CO.

Finally, as the temperature increases the quality of the produced gas yield improves, namely, the H_2 and CO yields, while the soot, tar and char yields decrease.

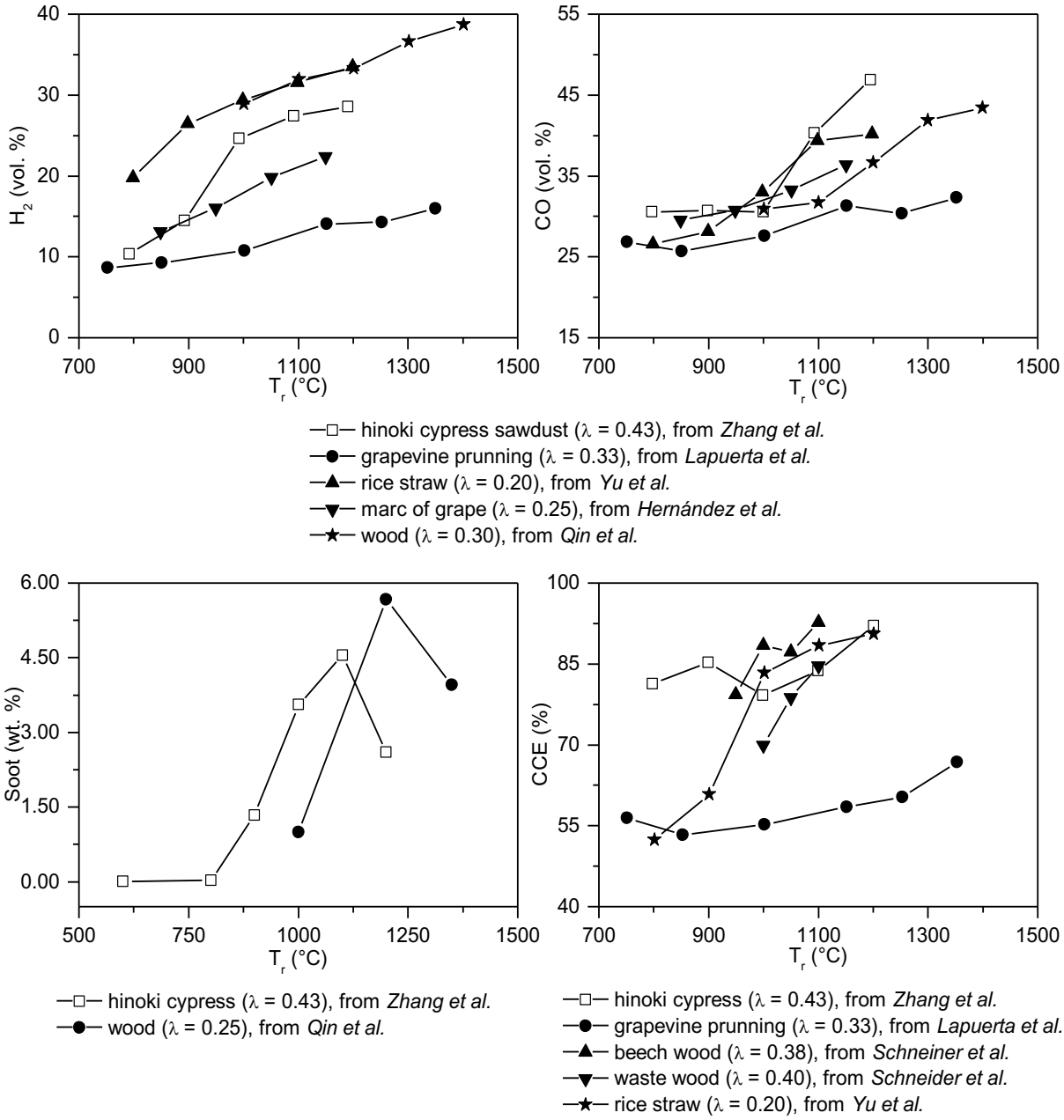

Figure I-9 - Effect of the temperature on the production of H_2 and CO, soot formation, and CCE during biomass gasification [38,42,44,46,47,49,50]**.**

I.2.2.2 Effect of the Gasifying Agent

The most widely used gasifying agents are air, carbon dioxide and steam. The influence of introducing oxygen (as air and steam) in the system have different effects [56]. As presented in Section I.2.1.1, oxygen is more reactive than steam, using less external heat to promote the process. A comprehensive study on the air influence is discussed in the following paragraphs.

The effect of excess air coefficient (λ) on biomass gasification process is a crucial parameter affecting the gas quality. Figure I-10 [43,46,47,49] shows results from the experiments performed by *Yu et al.* [46], *Lapuerta et al.* [47] and *Qin et al.* [43,49], who studied the impact of λ on the production of H_2 and CO, soot formation, and CCE during biomass gasification. Air was the oxidant used in all experiments, and the values of λ were achieved keeping the gas flow constant and changing the fuel feeding rate in order to keep other operating parameters nearly unchanged. The measurements were carried out with different biomass fuels, size ranges and temperatures.

The production of H_2 and CO decreased as the λ increased. Higher concentrations of oxygen in the process promotes the oxidation reactions (R_5, R_6, R_7 and R_8, Table I-2 [1]) consuming H_2, CO and carbonaceous gases, and forming mainly CO_2. The soot formation decreased with the increase of λ, due to the promotion of reaction R_5. These results are in agreement with the carbon conversion results. The carbon conversion increased with the increase of λ, indicating that higher values of oxygen in the process consumed more carbon from the fuel, corroborating with low formation of soot and char at higher λ values.

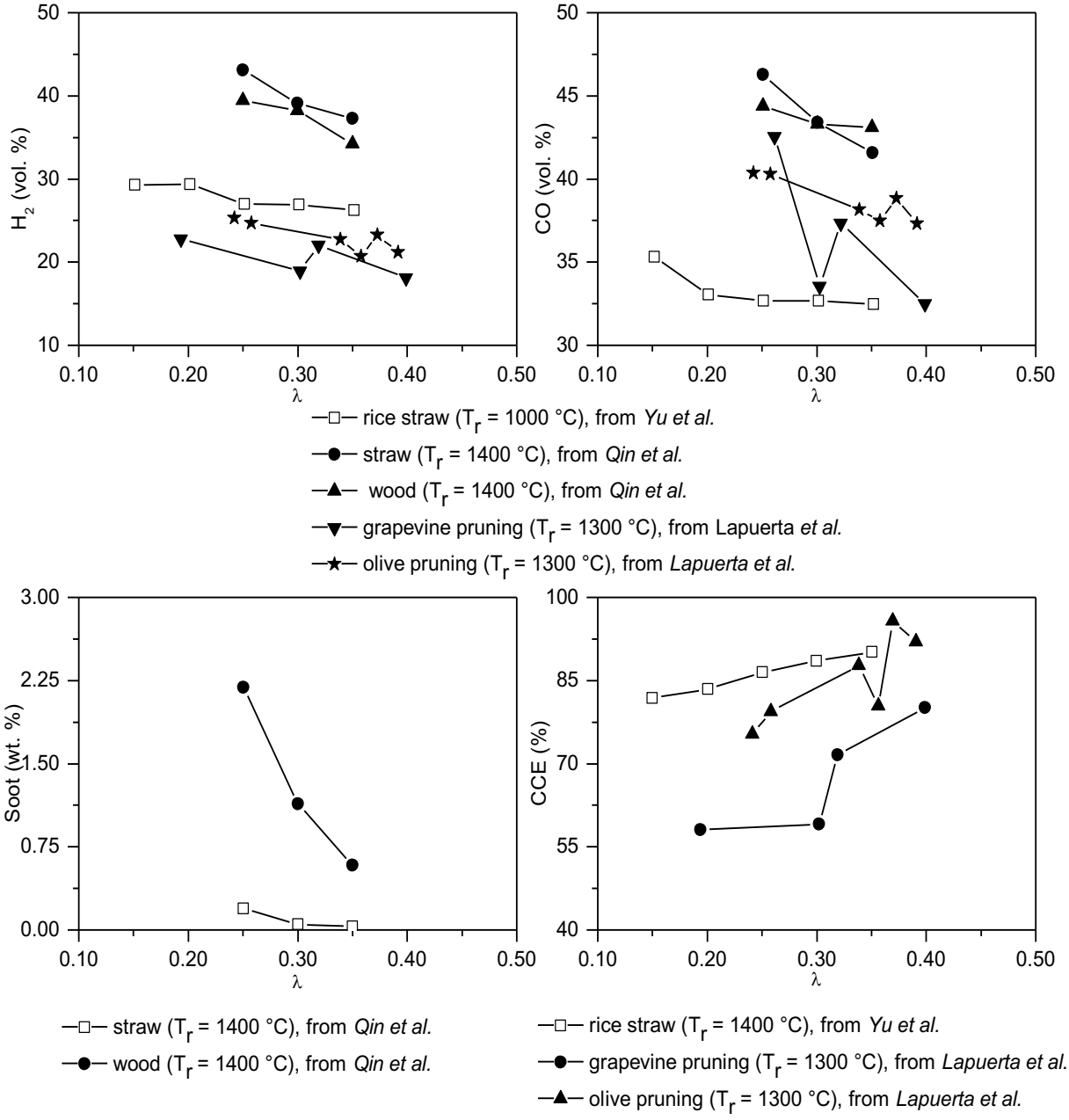

Figure I-10 - Effect of the λ on the production of H_2 and CO, soot formation, and CCE during biomass gasification [43,46,47,49]**.**

I.2.2.3 Effect of the Residence Time

Zhou et al. [48] studied the effect of the residence time (t_r) on the biomass gasification process, as shown in Figure I-11 [48]. All experiments were performed at a temperature of 1300 °C and an OB of 0.2. The biomass residues tested were rice husk and the camphor wood. The t_r was varied between 0.4 to 2 s by the variation of the carrier gas flow.

As t_r increased up to 1.2 s, the CO and CO_2 contents increased, the CH_4 content remained constant, and the H_2 content decreased. This is due to the lack of time for the biomass to be gasified, leaving

time for some oxidation. For t_r between 1.2 and 2 s, the H_2 and CO contents increased, the CH_4 content remained constant, and the CO_2 content decreased. This is due to more time remaining for the gasification to develop and generate more gaseous species. Higher values for t_r increased the CCE, as a result of a more complete gasification process.

Similar results were observed by *Hernández et al.* [50], who studied the effect of t_r from 1.36 to 1.92 s, at 1050 °C and for λ from 0.25 to 0.5 in the biomass gasification process.

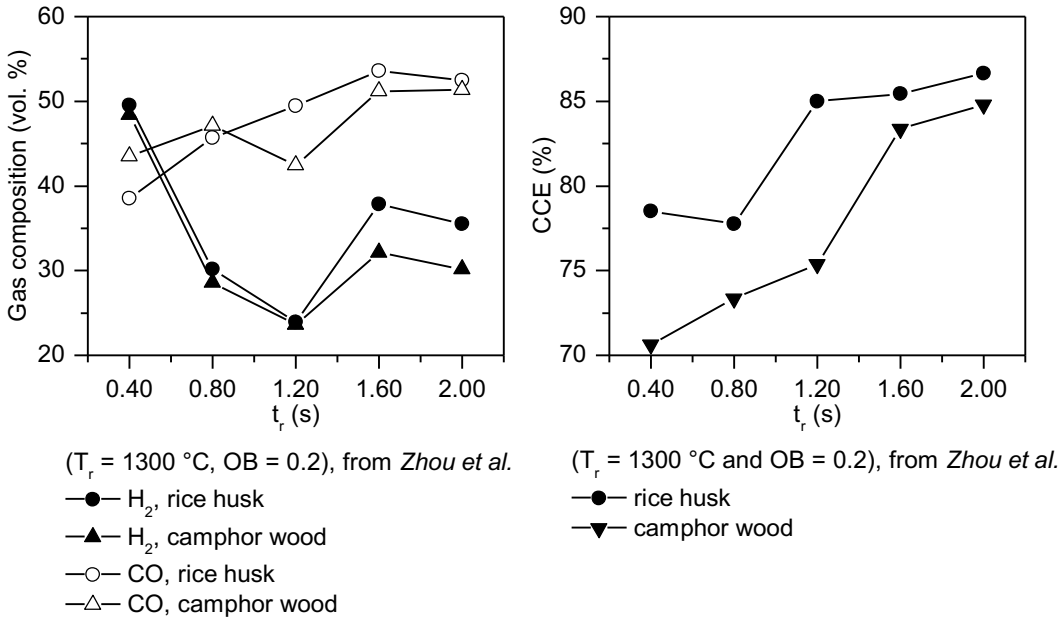

Figure I-11 - Effect of the residence time on the production of H_2 and CO, and CCE during biomass gasification [48].

I.2.2.4 Effect of the Particle Diameter

The effect of the particle diameter (d_p) on the gas composition and the CCE was studied by *Hernández et al.* [50], who performed biomass gasification tests with particles with a d_p from 0.5 to 8 mm, as shown in Figure I-12 [50]. The tests were carried out at a constant temperature of 1050 °C for a λ of 0.25.

While the particle size decreases, the H_2 and CO contents and the CCE increase. The smaller the particle is, the higher the area/volume, which promotes the release of more volatiles during the short period of pyrolysis and the char reactivity, leading to higher syngas quality. Also, smaller particles improve the mass and heat transfer, due to the lower diffusion resistance coefficients, which increases the reaction rate, improving also the syngas quality. Accordingly, smaller particles improve the main syngas characteristics and avoid blockage in the feeder, but may present technical and economical unfeasibility due to the difficulty and the increased grinding costs [33].

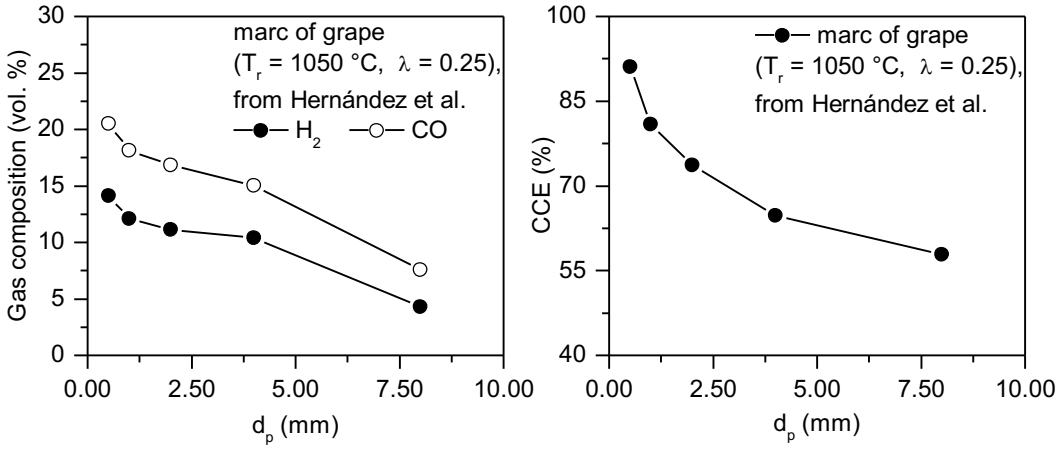

Figure I-12 - Effect of the particle size on the production of H_2 and CO, and CCE during biomass gasification [50]**.**

I.3 Objectives

The literature review shows that there is still the need to assess the biomass gasification behavior to understand the solid particle formation, namely soot and char formation, and the producer gas composition and quality under different operating temperatures. To this end, the first objective of the present work was to adapt the DTF from combustion to gasification. This new configuration needed to guarantee the control of the gasifying agent composition, solid particle sampling and syngas composition. The second objective was to carry out experiments at different operating temperatures at a constant excess air coefficient. The solid sampling gathered was analysed through SEM imaging and the syngas composition was determined with the aid of a GC. The data reported includes the weight and composition of the solid particle formation for four DTF operating temperatures (900, 1000, 1100 and 1200 °C), and gas composition and performance parameters (LHV, CGE, CCE and H_2/CO) for the same operating temperatures.

The specific research questions of this work are:

1. What is the impact of the operating temperature on the solid particle formation and syngas composition?
2. Which is the optimal operating temperature to produce a high-quality syngas?

I.4 Thesis Outline

The remainder of the present thesis is divided into three chapters. Chapter II describes the material and methods used to assess the technical aspects of the biomass gasification process in a drop tube furnace. Chapter III presents and discusses the influence of the operating temperature on the biomass gasification, namely on solid particles formation, gas composition and low heating value, carbon conversion efficiency, cold gas efficiency and hydrogen/carbon monoxide volume ratio. Finally, Chapter IV presents the main conclusions of this work and lists some suggestions for future research.

II. Material and Methods

II.1 Fuel Preparation and Characterization

Pulverized wheat straw pellets (WS) was chosen to perform this study. The raw biomass was pulverized with a 1-mm-diameter sieve using a laboratory-scale mill Retsch SM 100. The particles size used to perform this study is between 90 and 140 μm, obtained by using a SS-15 Gilson Economy 203 mm Sieve Shaker. The samples were stored in sealed containers to prevent oxidation, and were pre-processed to remove most of the moisture content by drying the samples at 105 °C for 2 h, as recommended by references [24,25]. The particle size distribution of the raw samples, illustrated in Figure II-1, was measured by the Malvern 2600 Particle Size Analyser. The median diameter (d_{50}) of the WS particles is 125 μm.

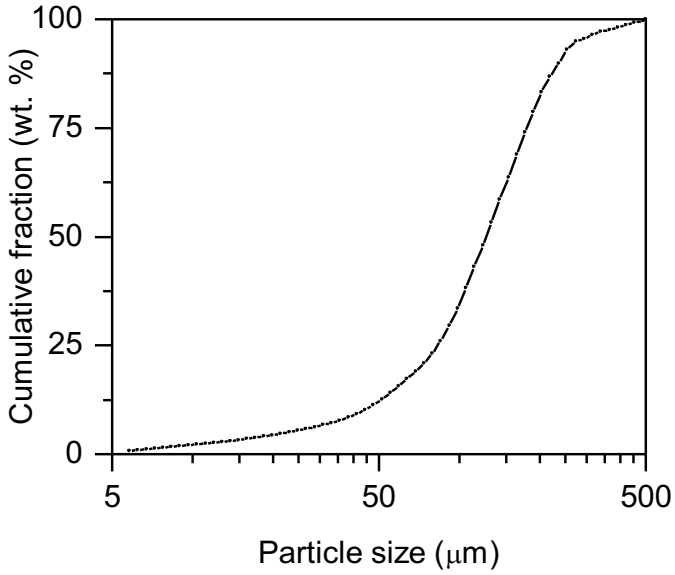

Figure II-1 - WS particle size distribution.

Table II-1 shows the properties of the biomass residue, including the ash composition. The ultimate analysis was determined accordingly to the standards CEN/TS 15104 and CEN/TS 15408 and the proximate analysis was determined following the procedures of the standards CEN/TS 15414:2006, CEN/TS 15402: 2006 and CEN/TS 15403:2006. The heating values of all the samples were determined following the procedures specified in the standards CEN/TS 14918:2015 and the chemical composition of the ashes was determined with the aid of x-ray fluorescence spectroscopy.

Table II-1 – WS ultimate, proximate and ash analysis.

Parameter	WS
Proximate analysis (wt.%, as received)	
Moisture	8.0
Volatile matter	64.9
Ash	14.7
Fixed Carbon (by dif.)	12.4
Heating value (MJ/kg, as received)	
Low	13.0
High	14.1
Ultimate analysis (wt.%, dry ash free)	
C	41.1
H	5.3
N	0.7
S	< 0.02
O (by dif.)	52.6
Ash analysis (wt.%, dry basis)	
Al_2O_3	8.7
CaO	28.0
Cl	0.6
Fe_2O_3	5.0
K_2O	6.9
MgO	3.7
Na_2O	0.6
P_2O_5	2.6
SO_3	1.0
Others	0.9

II.2 Experimental

II.2.1 Setup

Figure II-2 shows the schematic of the experimental setup used in the present study. The drop tube furnace gasification system is constituted by a fuel feeding system, gas (oxygen and nitrogen) supply system, vertical drop tube reactor, solid particle sampling system and gas sampling and analysis system.

The gasification chamber consists on a cylindrical electrically heated nonporous mullite tube with a total length of 1750 mm and inner diameter of 40 mm. It can reach a maximum temperature of 1300

°C. The furnace wall temperatures are continuously monitored using three thermocouples (type-K), equally spaced along the gasification chamber.

The feeding system is composed by a water-cooled injector, placed at the top end of the DTF, used to feed the fuel particles and the gasifying agent.

Upstream, the injector has a central pipe for the introduction of the pulverized biomass and transport fluid, and a concentric passage for the introduction of the secondary stream. A twin-screw volumetric feed transfers the biomass to an injector system from which the particles are gas-transported to the water-cooled injector. The transport fluid is nitrogen, and the secondary stream can be steam, oxygen, air, carbon dioxide and/or nitrogen. The nitrogen, carbon dioxide and oxygen are supplied from a bottle, the air is supplied by a compressor and the steam is produced by forcing distilled water through a steam generator. The steam generator, which is controlled by dedicated software, consists of a pressurized container with distilled water, water and gas flow meters, and a boiler. The container is pressurized up to 2 bar, the water flow meter measures up to 1200 g h^{-1}, the gas flow meter measures up to 80 L min^{-1}, and the boiler heats up to a temperature of 200 °C. The steam line is heated to a temperature of 200 °C in order to avoid water condensation. The remaining flow rates are controlled using manual flow meters.

Downstream, the particle collecting system is put into place. The particle collecting system is composed by an in-house made cyclone, a commercial (Dekati®) cyclone, metal filter, and vacuum pump. In the system, particles either fell down to the in-house made cyclone (see Section VI.1 for more details) or were separated using the Dekati® cyclone with a cut size of 10 μm. The Dekati® cyclone and the impactor were kept at a temperature of 150 °C by two Winkler heating blankets to minimize the condensation of liquids. Sampling was performed during 15 min, and after, the solid particles were collected, weighed and preserved for further analysis. The solid sampling started immediately after the measured gas composition reaches a stable state in the online analyser. The 15 min period of solid sampling was achieved after a comprehensive study in its influence (30, 25 and 20 min) on the impactor solid accumulation, where a 15 min showed almost no saturation.

The gas analysis of the desired gases (H_2, CO, CO_2 and CH_4) was performed with the aid of a gas chromatograph (GC).

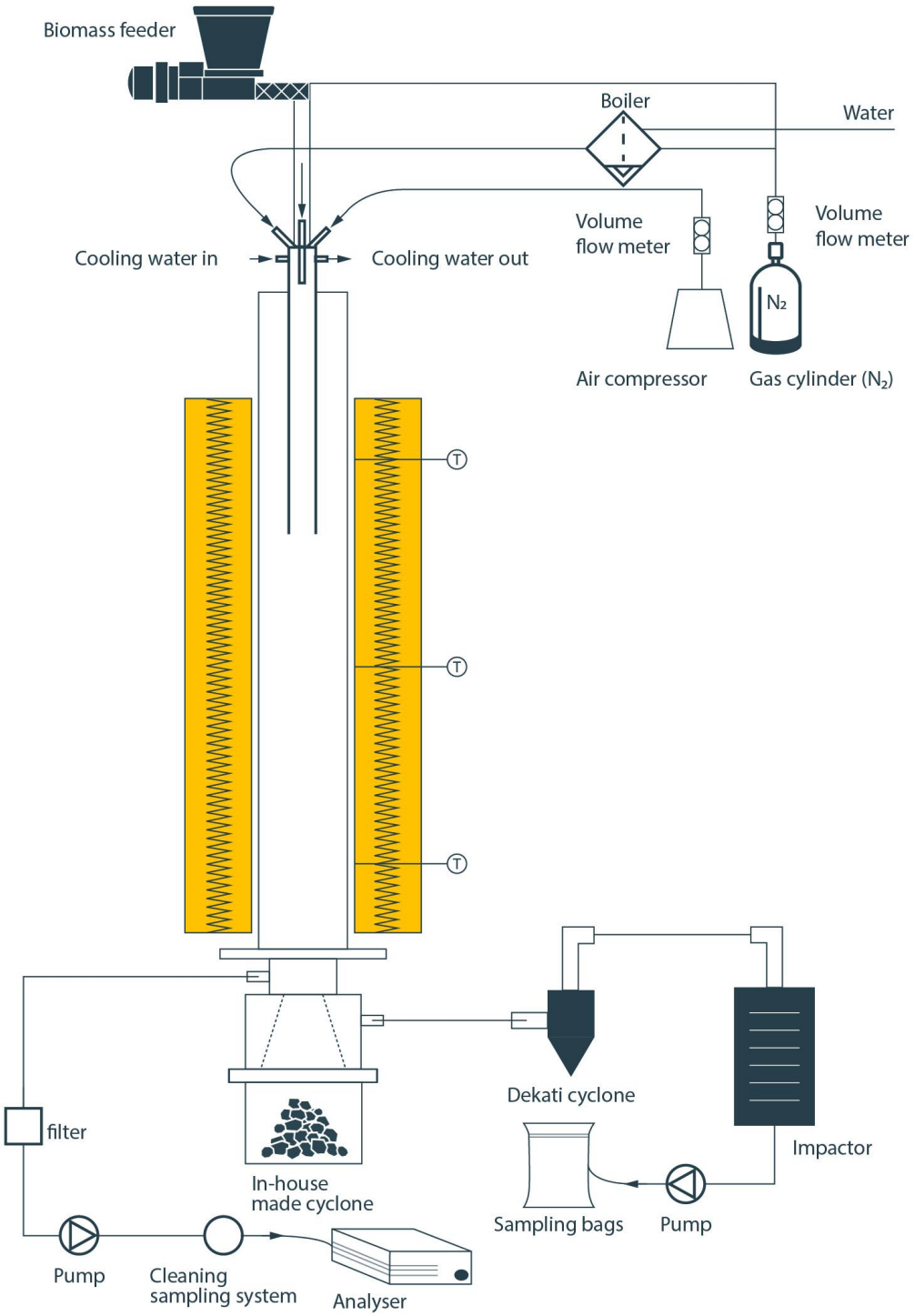

Figure II-2 - Schematic of the experimental setup.

II.2.2 Methods

Temperature Measurements

The local mean temperature measurements along the axis of the DTF were obtained using a 76 μm diameter fine wire type-R thermocouples (platinum/platinum-13 % rhodium). Figure II-3 illustrates the thermocouple probe used. The thermocouple hot junction was installed and supported by 350 μm wires of platinum/platinum-13 % rhodium located in a twin-bore alumina sheath with 5 mm of external diameter. The analogic outputs of the thermocouple were transmitted via an A/D board to a computer where the signals were processed, and the mean values computed.

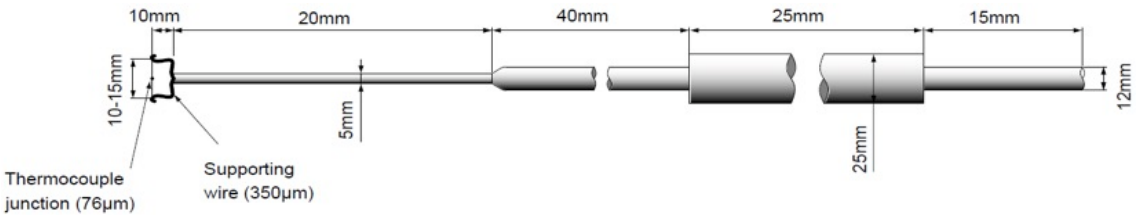

Figure II-3 - Thermocouple probe used for the temperature measurements along the DTF.

The temperature measured with an exposed thermocouple is biased by the furnace wall temperature, so that the real temperature was estimated based on an energy balance on the thermocouple bead [57]. The energy balance to the thermocouple bead neglects the heat transfer by conduction through the wires and the catalytic effects, so it only considers the balance between radiation and convection under steady state conditions, according to the following equations:

$$\dot{Q_{cond}} + \dot{Q_{cat}} + \dot{Q_{rad}} + \dot{Q_{conv}} = 0 \qquad (\mathrm{II}-1)$$

$$\varepsilon_t \sigma (T_t^4 - T_r^4) + h\left(T_t - T_g\right) = 0 \; with \; h = \frac{Nu\, k}{d_t} \qquad (\mathrm{II}-2)$$

Equation $(\mathrm{II}-1)$ is a simplified form of the Equation $(\mathrm{II}-2)$ with the considerations mentioned above.

Solid Samples

A cyclone was designed and produced in the workshop of the Mechanical engineering Department, to collect the largest particles (> 10 μm) at the bottom of the DTF. The cyclone, besides the solid collection, allows bypassing the solid samples system, in order to achieve a steady state before the solid sampling (see Section VI.1 for more details). Following the cyclone, the collected stream passed through a Dekati® cyclone, shown in Figure II-4 [58], where the remaining large solid samples were removed from the stream. The nominal gas flow through the cyclone was 10 L min^{-1} providing a cut

size of 10 μm. The temperatures in both cyclones did not fall below 150 °C. The finer solid samples, under 10 μm, were collected with the aid of the low pressure thirteen-stage cascade impactor (DLPI, Dekati® Ltd., shown in Figure II-5, left [58]), and illustrated schematically in Figure II-5, right [58]. The thinner particles pass through the nozzles of the jet plate with high speed and make a sharp turn to flow between the plates. Particles larger than a certain size cannot make the sharp turn and impact on the second plate. The nominal gas flow and low pressure through the cyclone and the cascade impactor were maintained with the help of a vacuum pump (115V/60 Hz IA-906 Dekati®) with a recommended flow rate of 10 L min^{-1} at 100 mbar [58].

Figure II-4 - Dekati® cyclone [58].

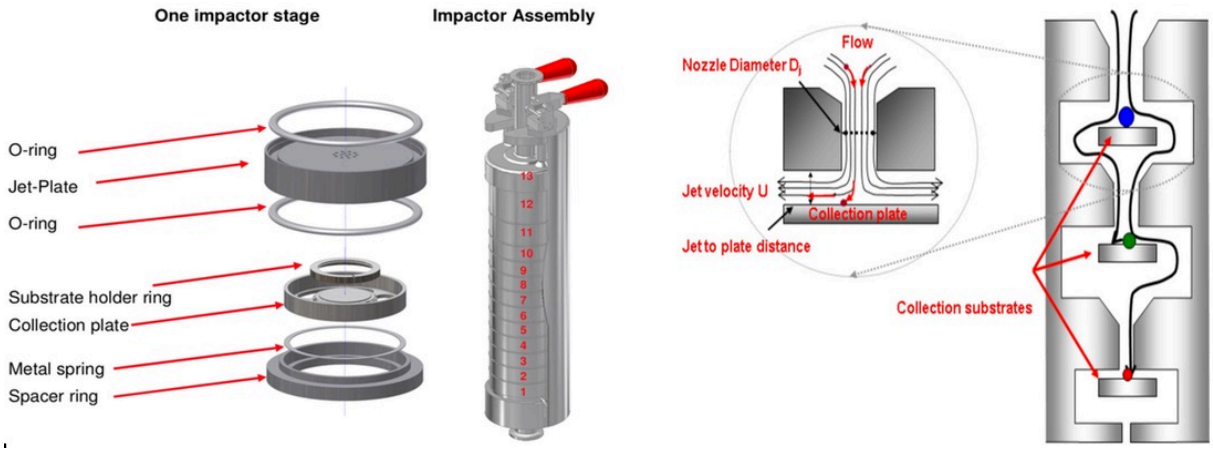

Figure II-5 – Dekati® cascade impactor (left) and the particle collecting mechanism (right) [58].

The DLPI allows the classification of small particles in different particle diameters according to Table II-2. PMs are collected on aluminum substrates of 25 mm diameter. The impactor was kept, during the whole experiment, at 150 °C by using a heating blanket (Wrinkler GmbH) to avoid gas condensation.

The substrates were weighted before and after each measurement in order to determine the PM formation.

Table II-2 - Particle diameter of each stage of the DLPI.

Impactor Stage	Aerodynamic Diameter (μm)
1	0.028
2	0.055
3	0.094
4	0.158
5	0.265
6	0.386
7	0.616
8	0.950
9	1.597
10	2.384
11	3.979
12	6.651
13	9.862

Chemical Species and Particle Morphology

Figure II-6 shows the SEM – Hitachi S2400 – facility used to evaluate the morphology, available in the Instituto Superior Técnico (IST) facilities, and the chemical composition of selected solid samples. The microscope is equipped with an energy dispersive x-ray spectroscopy (EDS) detector, which allows the quantification of the ultimate composition of a sample with a resolution of about 1 μm^2. For each selected PM sample (both cyclones and impactor substractes), chemical composition data, in terms of carbon, ashes and oxygen, was obtained from three different areas of about 50 x 50 μm^2 each.

Figure II-6 - Scanning electron microscope (SEM).

In order to use a larger amount of particles and have a overall look at the composition, a burnout was carried out. It consists in the burning of the particles up to 1100 °C in three different gradients over 15 hours. With the purpose of assess the composition in terms of ash and carbon. This temperature guarantees the evaporation of the carbon content. Based on the remaining solid sampling (i.e. ash) we were able to tell apart ash from carbon content in the samples.

Gas Composition

The gas products were collected in a SKC FlexFoil® sampling bags, at the end of the setup, after the vacuum pump (see Figure II-2).

The gas composition was measured using a GC, available in Universidade de Aveiro Departamento de Ambiente e Ornamento. The GC model used, was a SRI 8610C, equipped with a thermal conductivity detector (TCD) to measure light gases (e. g. H_2, CO, N_2 and CH_4). A 10-way valve with pneumatic control was used to automatize the process thus reducing the contamination from ambient air. It also eliminated human errors from manual injections, increasing drastically the repeatability of the data. The gas sample passed through a column, model MXT1, which is 1.60 m long, and a RTX Q-Plot, which is 2.15 m long. The column is a key element in GC, as depending on its active material, it will have different affinities with different elements. Separation of species is strongly influenced by the carrier gas and the column's active material. Temperature and carrier gas flow rate also influence the separation, and the temperature of the oven reached up to 140 °C and Argon (i.e. carrier gas) flow rate was limited to 20 mL min^{-1}.

II.3 Test Conditions

The WS feedstock particles ranged from 90 to 150 μm, and the feeding rate was fixed at 23 g h^{-1}. Experiments were carried out to stablish the influence of the temperature on the gasifying process. The operating temperature varied in intervals of 100 °C between 900 and 1200 °C and all the remaining operating parameters were kept constant. The tested conditions are listed in Table II-3. The solid sampling was performed during 15 min periods after reaching steady-state conditions.

Table II-3 - Experimental schedule for the study of the effect of the operating temperature.

Parameter	No.	d_p (μm)	T_r (°C)	λ	$\dot{m}_{N_2}$ (L min^{-1})
Temperature	1	90 – 150	900	0.40	10
	2	90 – 150	1000	0.40	10
	3	90 – 150	1100	0.40	10
	4	90 – 150	1200	0.40	10

III. Results and Discussion

This chapter presents the results and discussion of the influence of the operating temperature on the WS gasification process in the DTF. Table III-1 and Table III-2 show the results obtained during the study of the operating temperature. They contain the data for H_2, CO_2, CO, CH_4, soot and char yields, LHV, CGE (see Equation $(I-7)$) and CCE (see $(I-6)$).

A problem encountered during the syngas collection at 900 °C prevented the determination of the producer gas composition for this temperature. Nevertheless, for this temperature we were able to collect the solid sampling in the cyclones and the impactor.

Table III-1 - Results obtained for the H_2, CO_2, CO and CH_4 yields, LHV, CGE, CCE and H_2/CO in the study of the effect of the operating temperature ($\lambda = 0.4$).

T_r (°C)	H_2 (vol.%)	CO_2 (vol.%)	CO (vol.%)	CH_4 (vol.%)	H_2/CO	LHV (MJ kg^{-1})	CGE (%)	CCE (%)
1000	9.51 ± 2.01	48.36 ± 9.04	32.04 ± 3.21	10.09 ± 0.91	0.3 ± 0.07	8.69 ± 0.56	37.49 ± 4.9	66.15 ± 9.17
1100	17.85 ± 3.77	39.18 ± 7.36	33.33 ± 3.28	9.64 ± 0.89	0.54 ± 0.13	9.59 ± 0.67	48.95 ± 5.55	78.27 ± 10.42
1200	23.67 ± 4.95	38.04 ± 7.11	33.81 ± 3.38	4.48 ± 0.40	0.7 ± 0.16	8.43 ± 0.70	45.84 ± 6.73	83.35 ± 11.28

Table III-2 - Results obtained for the soot and char yields in the study of the effect of the operating temperature ($\lambda = 0.4$).

T_r (°C)	Soot (mg g^{-1}, db)	Char (mg g^{-1}, db)
900	3.08 ± 0.26	210.74 ± 12.01
1000	3.79 ± 0.32	194.18 ± 11.07
1100	3.20 ± 0.27	153.90 ± 8.70
1200	2.92 ± 0.25	133.48 ± 7.60

III.1 Drop Tube Furnace Gas Temperature Analysis

The gas temperature profiles along the height of the DTF are illustrated in Figure III-1. Six points were measured, with the insertion of the thermocouple, along the height of the DTF for four temperatures, 900, 1000, 1100 and 1200 °C. To replicate the working conditions, a flow of nitrogen and air was introduced while measuring of 10 L min^{-1} and 0.5 L min^{-1}, respectively. The results for each distance were obtained based on two measurements.

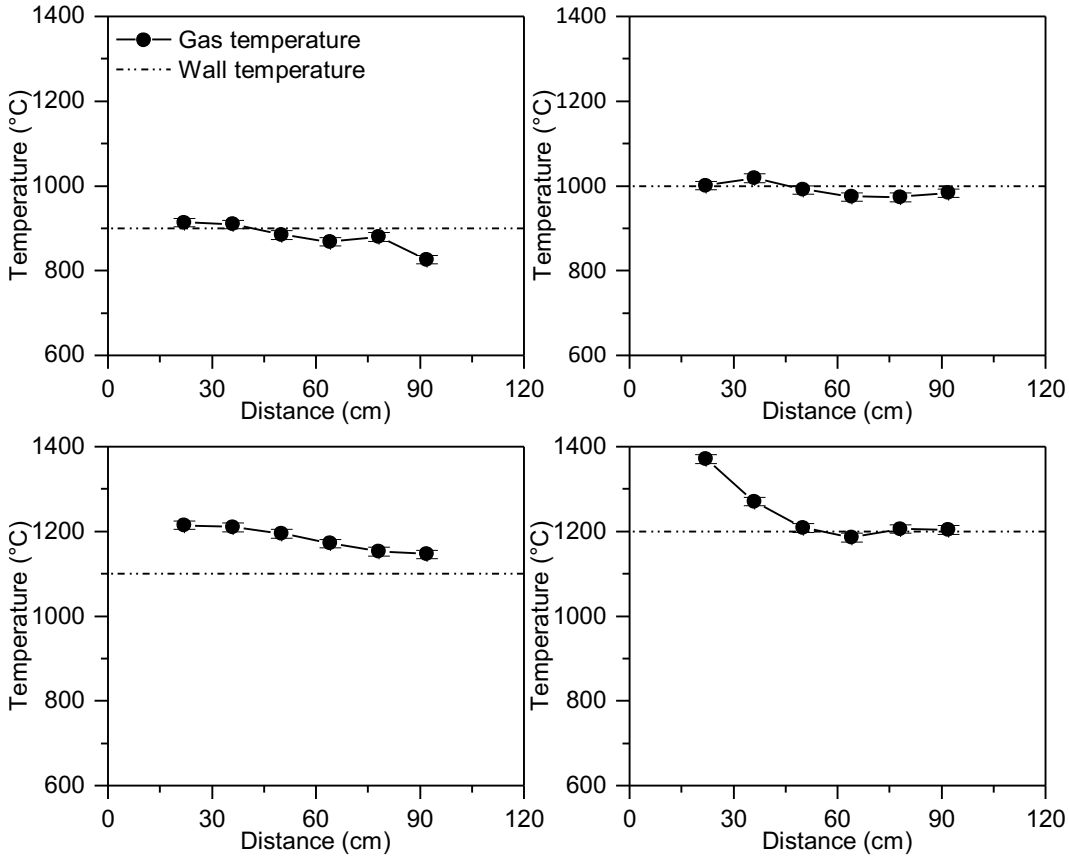

Figure III-1 -Gas temperature along the DTF at 900, 1000, 1100 and 1200 °C operating wall temperatures.

III.2 Producer Gas

The producer gas composition measured by the GC for the experiments were carried for operating temperatures of 1000, 1100 and 1200 °C.

The feeding rate of WS was 23 g h^{-1}. N_2 (i.e. carrier gas) and air (i.e. gasifying agent) were introduced in the system with flow rates of 10 L min^{-1} and 0.5 L min^{-1}, respectively. As result, the producer gas obtained was mainly formed by N_2 (~ 98 vol.%). Figure III-2 shows the evolution of the producer gas composition as a function of the operating temperature at a constant excess air coefficient. It contains the normalization of the valuable gases: CO, CO_2, CH_4 and H_2. Each experiment was repeated, at least, twice.

For the operating temperature between 1000 and 1200 °C, the H_2 yield significantly increased from 9.51 to 23.67 vol.%, while the CO yield slightly increased from 32.04 to 32.81 vol.%. CO_2 and CH_4 yields decreased from 48.36 to 38.04 vol.%, and from 10.09 to 4.48 vol.%, respectively.

It was established in previous studies that the effect of the temperature (see Section I.2.2.1) benefits endothermic reactions [38,42,44,46,47,49,50]. While the temperature increases, it promotes the reactions R_1, R_2 and R_3 (see Table I-2 [1]). The *Boudouard* reaction (R_1, Table I-2 [1]) produces CO consuming CO_2; the *Water-Gas* (R_2, Table I-2 [1]) and *Methane Steam Reforming* (R_{13}, Table I-2 [1])

reactions consume H_2O and CH_4 producing CO and H_2. This explains the global decrease in the CO_2 and CH_4 yields, and the increase in the H_2 and CO yields. Even though the CO content in the syngas slightly increased, being almost constant between 1100 °C and 1200 °C, it means that the CO production is reversed. It can be attributed to the WGS reaction (R_9, Table I-2 [1]), which is slightly exothermic and occurs easily, consuming CO and H_2O to produce H_2 and CO_2. This trend was previously observed in biomass gasification in air [42].

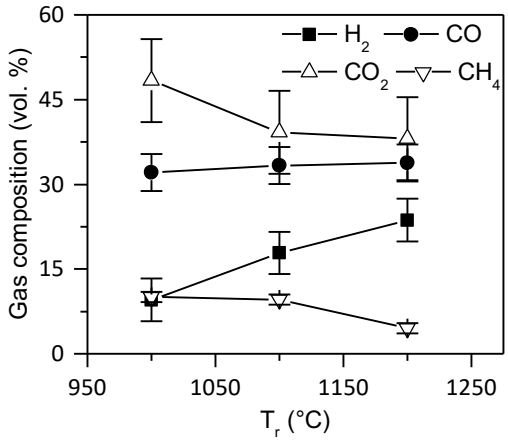

Figure III-2 - Effect of the operating temperature on the H_2, CO_2, CO and CH_4 yields ($\lambda = 0.4$).

These results reveal that as the operating temperature increases, the CO and H_2 yields increase, while the CO_2 and CH_4 yields decrease. However, in order to predict the optimum operating temperature, the LHV, the CGE, the CCE and the H_2/CO have to be examined as follows.

The producer gas is assessed based on the low heating value (LHV), cold gas efficiency (CGE), carbon conversion efficiency (CCE) and hydrogen/carbon monoxide ratio (H_2/CO). The heating value is the amount of heat produced by a complete combustion of fuel, the CGE determines the ratio of energy available in the syngas and the energy available in the biomass (see Equation $(I - 7)$), and the CCE is the ratio between the carbon in the syngas and the carbon introduced by the biomass (see Equation $(I - 6)$) [31]. Figure III-3 shows the effect of the operating temperature on the performance indicators (LHV, CGE, CCE and H_2/CO) at constant excess air coefficient.

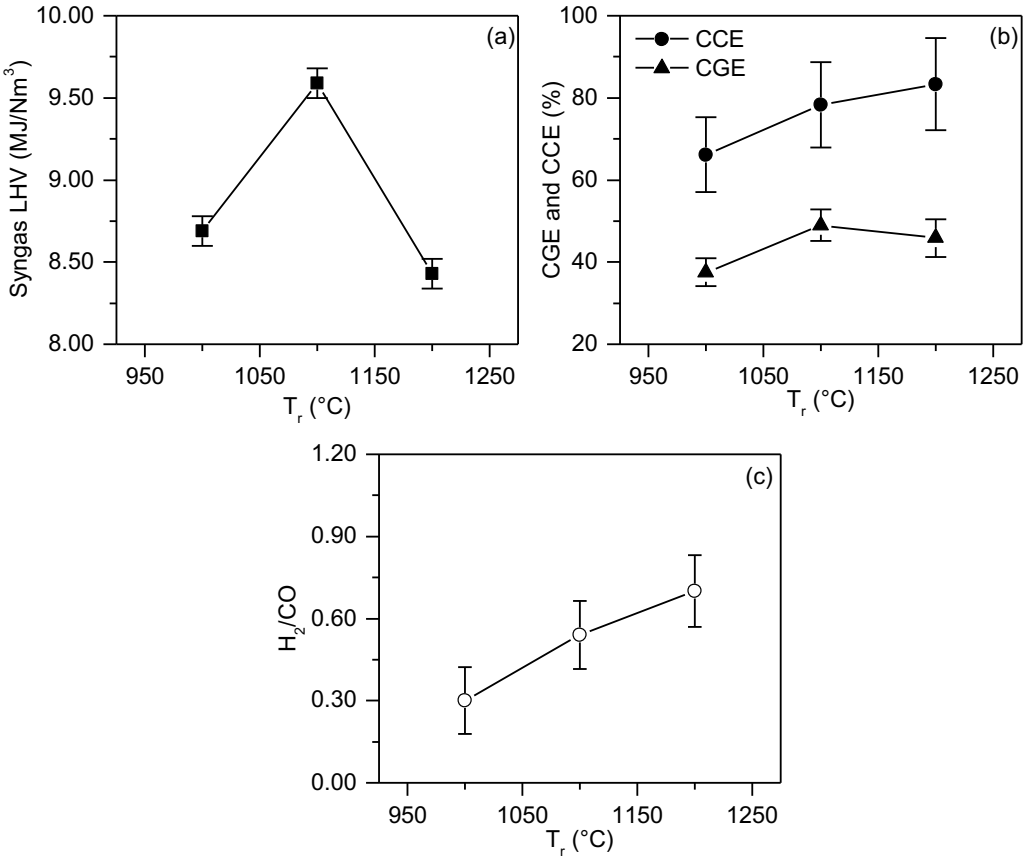

Figure III-3 - Effect of the operating temperature on gasification performance parameters ($\lambda = 0.4$): LHV (a), CGE and CCE (b) and H_2/CO (c).

The LHV of the producer gas was estimated considering the contribution of the CO, H_2 and CH_4 yields, introducing the calorific values from the company *TU Wien* presented in *Waldheim et al*. [59] (the LHV of CO, H_2 and CH_4 are 12.63, 10.783 and 35.88 MJ Nm^{-3}, respectively). It increased from 8.69 to 9.59 MJ Nm^{-3} for an operating temperature between 1000 and 1100 °C. This result could be attributed to the decrease of the CO_2 yield by approximately 9 vol.% as it reached 1100 °C. In fact, carbon dioxide is an inert gas that does not add calorific value to the syngas (the LHV of CO_2 is considered to be 0 MJ Nm^{-3}), so the producer gas at 1100 °C has less inert gas composition, increasing its LHV. Then, the syngas LHV decreased to 8.43 MJ Nm^{-3} at 1200 °C, due to the decrease by 6 vol.% of the CH_4 yield. Methane, as mentioned previously, has a higher LHV among all the constituents and, therefore, it has higher preponderance in the final result.

For operating temperatures between 1000 and 1100 °C, the CGE increased from 37.49 to 48.95%, and then it slightly decreased to 45.84 % at 1200 °C. The tendency to decrease at higher operating temperatures could be explained by the increase of the syngas yield not being able to compensate the decrease in the syngas LHV.

It was shown the continuous increase of the CCE over the operating temperature range studied. It increased from 66.15% to 83.35% as the operating temperature increased between 1000 and 1200

°C. The rapid increase of carbon conversion is well understood because, as the operating temperature increased, the overall PM formation decreases. This experimental observation, explains the promotion of the gasification reactions of carbon (R_1, R_2, R_3, R_4 and R_5, Table I-2 [1]). These results are consistent with those reported in the literature [38,42,44,46,47,49,50].

Due to the high increase in the H_2 yield and the nearly constant CO yield, the increase of the operating temperature between 1000 and 1200 °C enhanced the H_2/CO from 0.3 to 0.7. *Qin et al.* [49] and *Lapuerta et al.* [47] reported similar results.

The present results reveal that as the operating temperature increased, the H_2 and CO yields increased, while the CO_2 and CH_4 yields decreased. On the other hand, the CCE increased as the operation temperature increases, but the CGE presented a maximum value at 1100 °C. Nevertheless, the operating temperature has a limited effect on the LHV, since it varies less than two units while the operating temperature shifts. In order to select an optimal biomass gasification operating temperature, the final application of the syngas must be identified, as is discussed in Section III.4. The operating temperature for an optimal high-quality producer gas to be used in energy production seems to be 1100 °C. It leads to a CCE of 78.27%, and to the highest values of LHV and CGE of 9.59 MJ Nm^{-3} and 48.95%, respectively. Also, it corresponds to a reasonable value for the H_2/CO ratio, since it increased only by approximately 0.14, between an operating temperature of 1100 and 1200 °C.

III.3 Particulate Matter Production

PMs in the gasification process can be assumed to be formed of char and soot. But, as a first step, they will be separated into two size categories. Fine particles, with a diameter smaller than 10 μm, captured in the impactor (DLPI), and large particles with a diameter larger than 10 μm, collected in both the in-house made cyclone, and the Dekati® cyclone. In the following paragraphs, both the in-house made cyclone and the Dekati® cyclone will be referred to as “cyclone”. Each experiment was repeated, at least, twice.

Figure III-4 illustrates the influence of the operating temperature on the formation of PMs in the cyclone and the impactor. The amount of PMs collected in the cyclone decreased from 208.7 to 133.3 mg g^{-1}, db, as the temperature increased from 900 to 1200 °C. On the other hand, in the impactor, the quantity of PMs increased from 5.13 to 6.15 mg g^{-1}, db, between 900 and 1000 °C, where it reached its maximum at 1000 °C. Then, it decreases until 1200 °C reaching 3.10 mg g^{-1}, db.

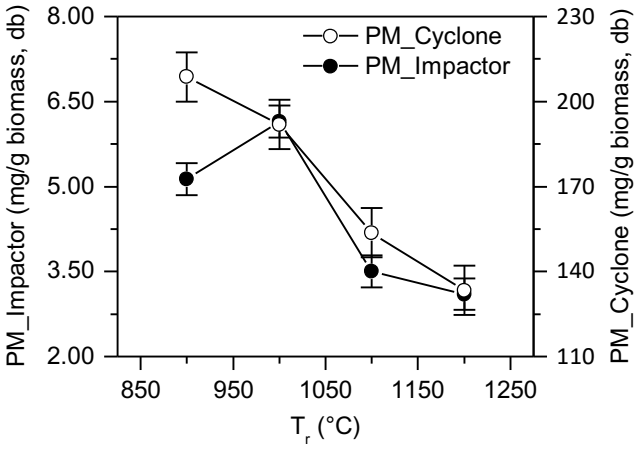

Figure III-4 - Effect of the operating temperature on the PMs collected in the cyclones and impactor ($\lambda = 0.4$).

As observed by *Kurian* et al. [28], soot particle diameter varies from 10 to 50 nm, and may reach a size up to 200 nm when agglomerated. As described in Section 0, the stage 5 of the impactor has a cut size of 265 nm. Thus, it could be assumed that the stages between 6 and 13 are likely to be char. Nevertheless, a further analysis of PM samples was used to identify and confirm the formation in the solid sampling of soot and char, as discussed in the following paragraphs.

III.3.1 Particulate Matter in the Cyclone

SEM and EDS analysis were performed on PMs collected in the cyclone at 900, 1000, 1100 and 1200 °C. For each selected sample in the EDS, the chemical composition data was obtained from three different areas of about 50 x 50 μm^2 each. Also, it was performed a burnout experiment to consolidate the EDS results. It consists in burning a PM sample overnight in order to keep the inorganics only (i.e. ash). The sample is weighted before and after burning; the difference is considered to be the organic material (i.e. carbon). SEM, EDS and burnout results for the cyclone at the operating temperatures of 900 and 1000 °C are presented in Table III-3.

For all temperatures studied, the SEM images are quite similar showing particles of 100 μm and different geometrical forms. Since soot aggregates generally in particles with approximately 200 nm, the PMs collected in the cyclone could be just char particles. These results are supported by the burnout experiment and the EDS analysis. For an operating temperature of 1000 °C, the burnout experiments showed a sample constituted of 65 wt.% of carbon and 35 wt.% of ash. The regions analysed by the EDS have a content of 61 wt.% of carbon, 22 wt.% of oxygen and 17 wt.% of ash. When normalized, it reached a composition of 78 wt.% of carbon and 22 wt.% of ash. The ash chemical composition showed is mainly formed by Ca, K and Si, and contains Mg, Al, Cl and Fe, as expected, due to the properties of the biomass (Table II-1). The difference between the EDS and burnout results can be attributed to the measuring techniques. A large fraction of the PMs collected in the cyclone was used to perform the burnout experiment, whereas only a small portion was used in

the EDS, and an even smaller portion was analysed. The EDS results are accurate locally, so there is the need to account for a margin of error when analysing it globally. The same assumption can be made about the PMs collect in the cyclone at 900 °C.

Even though char and soot are mainly formed by carbon, according to the literature (see Section I.2.1.1), soot is formed by approximately 90 wt.% of carbon [28]. Therefore, the chemical composition of the samples leans more towards char particles, because soot is expected to have higher carbon content. Thus, it is possible to confirm that the PMs collected in the cyclone are essentially char particles.

III.3.2 Particulate Matter in the Impactor

For the DLPI impactor, the PMs collected in the thirteen-stages at 1000 °C went through a SEM and EDS analysis. The burnout experiment could not be accomplished correctly, since the filter presents a substrate on its bed, leading to an excess matter not accountable in the burnout. The SEM and EDS analysis for the PM in the impactor are presented in Table VI-1 (see Section VI.2). EDS results for the stages 3, 4, 5 and 10 of the impactor differed from the remaining stages.

SEM observations showed that as the stages decrease the particles have a smaller size. Also, between stage 10 and 13, the PMs are randomly shaped and are composed by 59 to 69 wt.% of carbon, 22 to 28 wt.% of oxygen and 9 to 13 wt.% of ash. These results are quite similar to the results from the PMs collected in the cyclone (see Section III.3.1). Thus, it can be assumed the particles from the stages 10, 11, 12 and 13 are essentially char.

As stage 9 is reached, its noticeable the agglomeration of spherules in the SEM images. The agglomerations were smaller than 200 nm, and it was possible to observe in stages 2 and 1 spherules of approximately 50 nm of diameter. These observations were very similar to those in the literature, for a typical soot particle sample (see Figure I-5 [9,10], right). In addition, between stages 10 and 9, the carbon content in the PMs increased significantly, as shown by the EDS analysis. The new range of chemical compositions for stages 1 to 9 is: 81 to 86 wt.% of carbon, 3 to 11 wt.% of oxygen and 8 to 16 wt.% of ash. The ash chemical composition showed is mainly formed by Ca, K and Si, and contains Mg, Al, Cl and Fe, as expected, due to the chemical properties of the biomass ash (Table II-1). These carbon compositions were closer to soot than the cyclone PMs. Therefore, SEM, EDS and burnout analysis, enabled to identify char and soot properly. Char was collected in the cyclone and stages 13, 12, 11 and 10 of the impactor, whereas soot was collected in stages 1 to 9 of the impactor.

Table III-3- SEM images and EDS and burnout analysis for the PMs collected in the cyclone at 900 and 1000°C ($\lambda = 0.4$).

T_r (°C)	SEM Image	EDS Analysis	Burnout Experiment
900	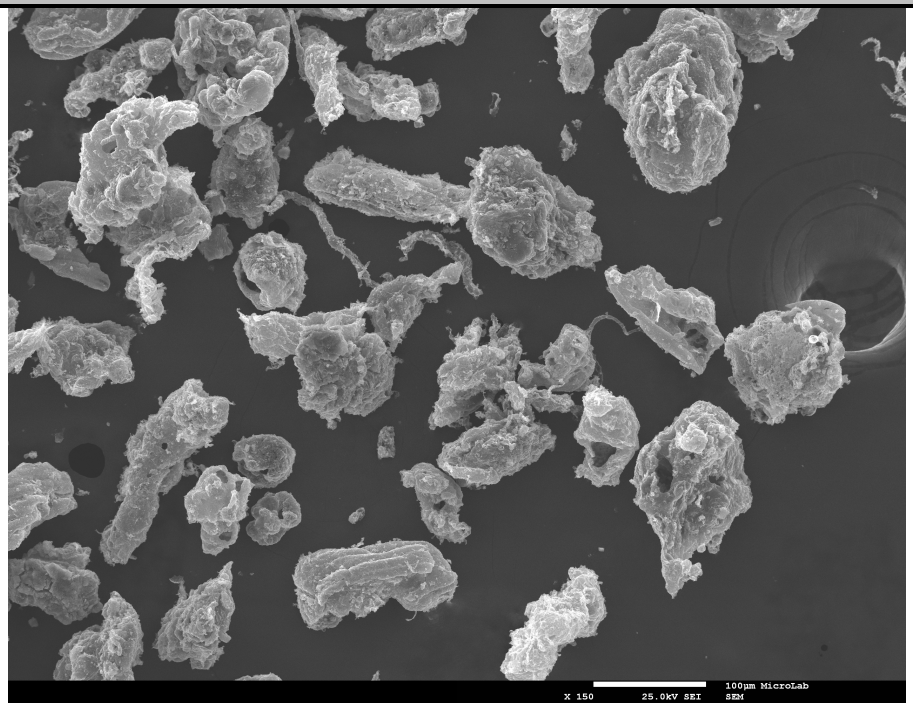	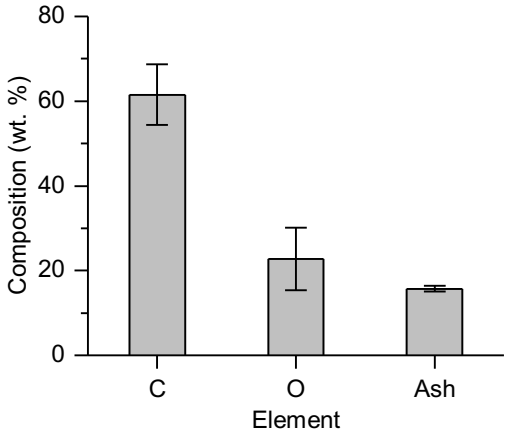	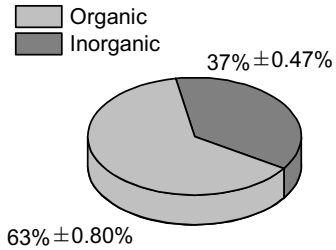

T_r (°C)	SEM Image	EDS Analysis	Burnout Experiment
1000	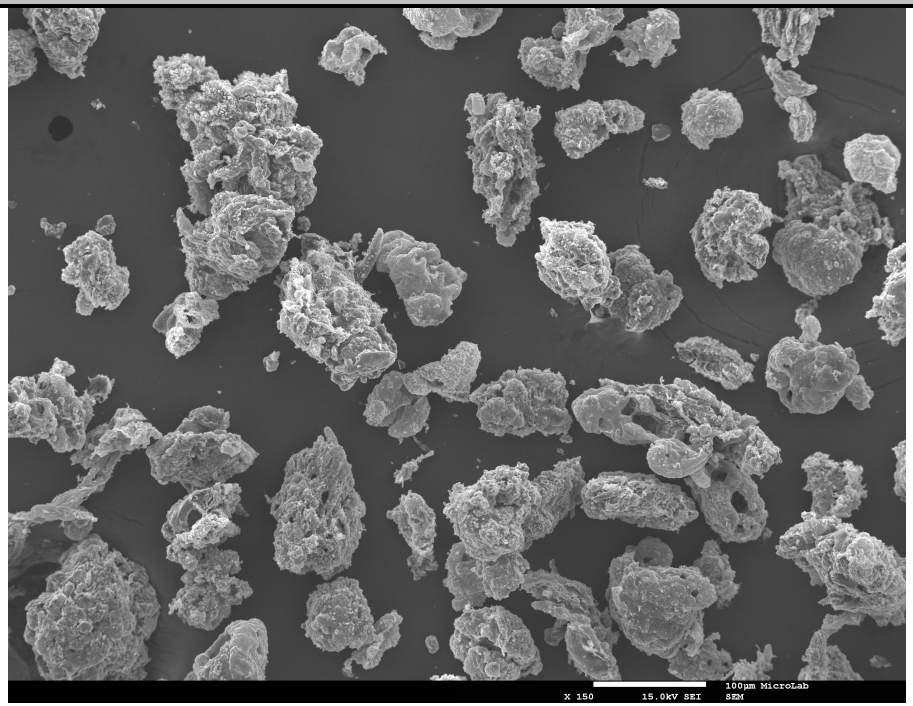	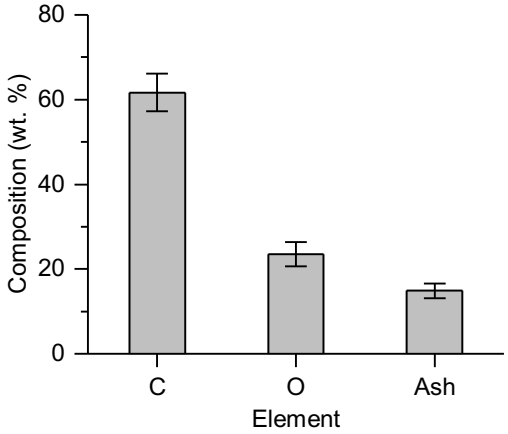	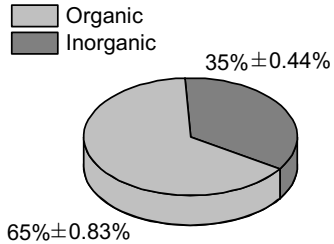

III.3.3 Char and Soot Formation

Based on the identification, previously presented, a final distribution of PMs can be made. Figure III-5 plots the effect of the operating temperature on the formation of char and soot.

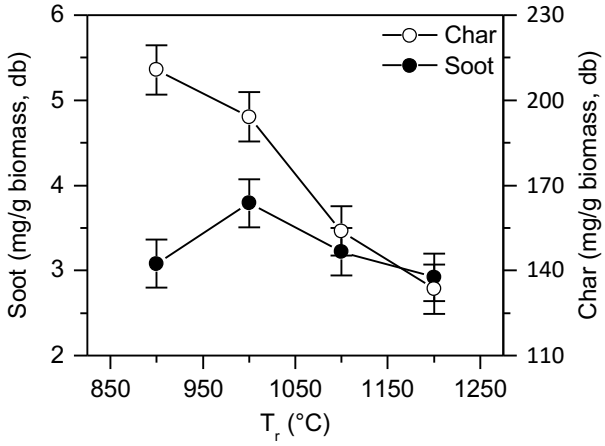

Figure III-5 – Effect of the operating temperature on soot and char formation ($\lambda = 0.4$).

Higher operating temperatures had a positive effect on char destruction. For instance, char formation decreased from 210.74 mg g^{-1}, db, at 900 °C to 133.48 mg g^{-1}, db, at 1200 °C. Soot formation first increased between 900 °C and 1000 °C, reaching a peak at 1000 °C (3.79 mg g^{-1}, db). As the temperature increased to 1200 °C, the soot decreased to 2.92 mg g^{-1}, db. Similar results were already published [43,44]. Finally, volatiles (i.e. producer gas) yield increased with the increment of the operating temperature and reached its maximum of 86.36 wt.% at 1200 °C. This operating temperature corresponded to the lowest values of char and soot of 13.35 wt.% and 0.29 wt.%, respectively. By difference of the solid formation, its possible to assess that the increase of the operating temperature has a positive effect in the volatile formation.

These results unfold that lower temperatures, such as 900 and 1000 °C, present higher values for char and soot formation. On the other hand, higher temperatures lead to a higher producer gas yields, and decreases the formation of char and soot yields. As inferred before, 1100 °C appears to be the most suitable operating temperature for an optimal high-quality producer gas to be used in energy production, in consideration of the lower char and soot formation, and higher values of LHV, CGE, CCE, and the H_2 and CO yields.

III.4 Practical Implication of this Work

The work developed aimed to study the syngas quality, based on indicators, such as syngas composition and its solid matter formation. In order to identify the optimal operating temperature, some factors must be accounted for such as soot formation, syngas yield and syngas cleaning technologies, along with the identification of the syngas final application.

First of all, the gasification process promotes the formation of soot, and, in this work, produces a low quantity of syngas (~ 2 vol.%), when compared with the carrier gas (~ 98 vol.% of nitrogen). The formation of soot is a highly undesirable by-product for downstream applications, such as turbines. The soot content in the syngas can affect the turbine durability and integrity, carbon deposition and smoke emissions, lowering the turbine performance [14,15]. Thus, temperatures above 1000 °C should be considered, to minimize the formation of PMs. Both soot and char formation decrease at higher temperatures. Temperatures below 1000 °C should consider a particle cleaning system technology, such as inertial separation, barrier filtration and electrostatic separation [60], which, depending on purity requirement, can be very costly. On the other hand, the syngas obtained is a small fraction of the output gas, leading to two constrains. First, the need to isolate the nitrogen to avoid pollutants, such as the formation of nitric acids, and, second, the industrial application is restricted, due to the low syngas production. Regardless of the industrial application, this work provides a reasonable contribution to the fundamentals of biomass gasification.

Finally, the syngas can have distinct downstream applications and must take into account the factors previously considered. For instance, at low operating temperatures the producer gas should aim to produce synthetic natural gas, due to a methane content promotion, but the low temperatures promote the formation of char as well. Char may increase the fertility and stability of soils, and can behave as carbon dioxide sequester, due to its carbon and ash content. Nevertheless, higher temperatures increase the performance indicators H_2/CO, LHV, CGE and CCE. At 1200 °C the ratio between hydrogen and carbon monoxide is the highest, suggesting relevance to the chemical industries; in particular, for the methanol and ammonia industries, since the main resources for their production are hydrogen and carbon monoxide, and hydrogen and nitrogen, respectively [61]. An operating temperature of 1100 °C is the most suitable for the use of the syngas for energy production in engines and turbines, as a result of the highest LHV, CGE and reasonable values for CCE, and H_2 and CO yields.

IV. Conclusion and Future Work

IV.1 Conclusion

Several experiments have been carried out in the drop tube furnace using pulverized WS as fuel in order to ascertain the effect of the operating temperature on the gasification process.

This study shows that the increase in the operating temperature has a positive effect on volatile formation and char destruction. These results are in accordance with the gasification reactivity, since heterogeneous reactions improve with the increase in the operating temperature. On the other hand, soot formation increases until it reaches a maximum at 1000 °C, temperature above which it starts to decrease. Since soot is a highly undesirable pollutant, WS gasification should be performed at operating temperatures above 1000 °C.

Results also indicate that higher operating temperatures result in higher CO and H_2 yields, higher carbon conversion efficiency and higher H_2/CO, but lower yields of CH_4 and CO_2. Higher temperatures benefit endothermic reactions, which promotes the formation of CO and H_2, and the consumption of solid carbon, CH_4 and CO_2. However, operating temperatures seem to have little influence on the producer gas low heating value, which varies by less than two units with operating temperature variations. At the temperature of 1100 °C, both low heating value and cold gas efficiency present a maximum value. The low heating value and the cold gas efficiency decrease at higher temperatures, since the CH_4 content decreases with the temperature, and the syngas gas yield increase cannot compensate the decrease in the low heating value, respectively.

The answers to the two specific research questions are as follows.

1. The increase of the operating temperature decreases the formation of char particles. Higher operating temperature promotes heterogeneous reactions, leading to a decrease from 210.74 mg g^{-1}, db, at 900 °C to 133.48 mg g^{-1}, db, at 1200 °C. Soot formation shows a maximum at 1000 °C of 3.79 mg g^{-1}, db, and 2.92 mg g^{-1}, db, at 1200 °C. Higher operating temperatures improved the H_2 and CO yields, and reduced the CO_2 and CH_4 yields, since it enhances the endothermic reactions.
2. To assess the optimal operating temperature for a high-quality syngas, the final downstream application of the syngas must be identified. The results showed that lower operating temperatures point to the production of synthetic natural gas and fertilization or soil amendment, since it promotes the formation of methane and char, being 10.09 vol.% and 210.74 mg g^{-1}, db, respectively. It suggested as well, for an operating temperature of 1200 °C, relevance to the chemical industry for the production of methanol and ammonia, since the syngas have a H_2/CO ratio of 0.7. At 1100 °C, the experiment showed higher values for the LHV and CGE, of 9.59 MJ Nm^{-3} and 48.95%, respectively, and reasonable values of 78.27% for the CCE and 0.54 for H_2/CO, producing a high-quality syngas for energy production applications.

IV.2 Future Work

During this master thesis, the impact of the operating temperature on the syngas quality was investigated. It will be interesting to study the effect of other operating parameters, such as the type of biomass, the biomass particle size, the residence time, impregnation of biomass with inorganics such as potassium, or the use of steam and carbon dioxide as gasifying agent. Steam leads to a richer producer gas in H_2, since it promotes de *WGS* reaction to the formation of H_2 and CO_2. Moreover, carbon dioxide promotes the *Boudouard* equation, enhancing the formation of CO. However, both being less reactive than oxygen, it requires more external heat supply and could lead to more costs. Using a blend of steam, air and carbon dioxide could significantly decrease the cost and still increase the gasification efficiency and the producer gas yield.

On the other hand, tar is a black and viscous product of the gasification that obstructs the equipment. It could be interesting as well to study tar formation and composition in the gasification process. Notwithstanding, the syngas must go through a cleaning process before the downstream application. An additional investigation on syngas cleaning technologies is interesting. It could be used to clean-up and separate the desired gases, such as methyl diethanolamine or methanol.

V. References

[1] P. Basu, Biomass gasification and pyrolysis: Practical design and theory, 1st ed., Elsevier Inc., 2010.

[2] G.J. Stiegel, M. Ramezan, Hydrogen from coal gasification: An economical pathway to a sustainable energy future, Int. J. Coal Geol. 65 (2006) 173–190. doi:10.1016/j.coal.2005.05.002.

[3] C. Higman, Syngas Database: 2017 Update, 2017.

[4] C. Higman, S. Tam, Advances in coal gasification, hydrogenation, and gas treating for the production of chemicals and fuels, Chem. Rev. 114 (2014) 1673–1708. doi:10.1021/cr400202m.

[5] G.J. Stiegel, Overview of gasification technologies, National Energy Technology Laboratory, 2005.

[6] WBA global bioenergy statistics, World Bioenergy Association, 2016.

[7] D.J. Stevens, Hot gas conditioning: Recent progress with larger-scale biomass gasification systems; Update and summary of recent progress, Technical Report, 2001. doi:10.2172/786288.

[8] M. Costa, P. Coelho, Combustão, 2nd ed., Orion, 2012.

[9] B. Demirdjian, D. Ferry, J. Suzanne, O.B. Popovicheva, N.M. Persiantseva, N.K. Shonija, Heterogeneities in the microstructure and composition of aircraft engine combustor soot: Impact on the water uptake, J. Atmos. Chem. 56 (2007) 83–103. doi:10.1007/s10874-006-9043-9.

[10] V.S. Chithra, S.M. Shiva Nagendra, Chemical and morphological characteristics of indoor and outdoor particulate matter in an urban environment, Atmos. Environ. 77 (2013) 579–587. doi:10.1016/j.atmosenv.2013.05.044.

[11] T.C. Bond, S.J. Doherty, D.W. Fahey, Bounding the role of black carbon in the climate system: A scientific assessment, J. Geophys. Res. Atmos. 118 (2013) 5380–5552. doi:10.1002/jgrd.50171.

[12] R. Agarwal, A. Awasthi, N. Singh, S.K. Mittal, P.K. Gupta, Epidemiological study on healthy subjects affected by agriculture crop-residue burning episodes and its relation with their pulmonary function tests, Int. J. Environ. Health Res. 23 (2013) 281–295.

doi:10.1080/09603123.2012.733933.

[13] V. Lopes, Effect of Particle Size on the burnout and emissions of particulate matter from biomass combustion in a drop tube furnace, MSc Thesis, Instituto Superior Técnico, 2016.

[14] Y.S.H. Najjar, R.M. Droubi, Soot formation in gas turbine combustors, Fuel Sci. Technol. Int. 5:4 (1987) 373–386. doi:10.1080/08843758708915859.

[15] R.K. Mishra, S. Chandel, Soot formation and its effect in an aero gas turbine combustor, Int. J. Turbo Jet Engines. (2016). doi:10.1515/tjj-2016-0062.

[16] United States Environmental protection agency, 2018. https://www.epa.gov/clean-air-act-overview (accessed June 7, 2018).

[17] J. Rezainyan, N. Cheremisinoff, Gasification Technologies A Primer for Engineers and Scientists, 1st ed., CRC Press, 2005.

[18] K. Littlewood, Gasification: Theory and application, Prog. Energy Combust. Sci. 3 (1977) 35–71. doi:10.1016/0360-1285(77)90008-9.

[19] S.K. Sansaniwal, K. Pal, M.A. Rosen, S.K. Tyagi, Recent advances in the development of biomass gasification technology: A comprehensive review, Renew. Sustain. Energy Rev. 72 (2017) 363–384. doi:10.1016/j.rser.2017.01.038.

[20] C. Higman, M. Van Der Burgt, Gasification, 2nd ed., Gulf Professional Publishing, 2008. doi:10.1016/B978-0-7506-8528-3.00002-X.

[21] L. Klass, D, Biomass for renewable energy, fuels, and chemicals, 1st ed., Academic Press, 1998.

[22] H. Knoef, Handbook biomass gasification, 2nd ed., BTG Biomass Technology Group, 2012. http://gen.lib.rus.ec/book/index.php?md5=46B009D73BA3F11158A040EDA5444D53.

[23] P. Mckendry, Energy production from biomass (part 1): Overview of biomass, Bioresour. Technol. 83 (2002) 37–46. doi:10.1016/S0960-8524(01)00118-3.

[24] J.G. Brammer, A. V. Bridgwater, The influence of feedstock drying on the performance and economics of a biomass gasifier - Engine CHP system, Biomass and Bioenergy 22 (2002) 271–281. doi:10.1016/S0961-9534(02)00003-X.

[25] H. Kumar, P. Baredar, P. Agrawal, S.C. Soni, Effect of moisture content on gasification efficiency in down draft gasifier, Int. J. Sci. Eng. Technol. 3 (2014) 411–413.

[26] A. Kumar, D.D. Jones, M.A. Hanna, Thermochemical biomass gasification: A review of the

current status of the technology, Energies 2 (2009) 556–581. doi:10.3390/en20300556.

[27] C. Di Blasi, Combustion and gasification rates of lignocellulosic chars, Prog. Energy Combust. Sci. 35 (2009) 121–140. doi:10.1016/j.pecs.2008.08.001.

[28] V. Kurian, Asphaltene gasification : Soot formation and metal distribution, University of Alberta, 2016.

[29] J. Ma, Soot formation during coal pyrolysis, PhD Thesis, Brigham Young University, 1996.

[30] A.F. Sarofim, J.P. Longwell, M.J. Wornat, J. Mukherjee, The role of biaryl reactions in PAH and soot formation, Springer Berlin Heidelberg, 1994. doi:10.1007/978-3-642-85167-4_27.

[31] M. La Villetta, M. Costa, N. Massarotti, Modelling approaches to biomass gasification: A review with emphasis on the stoichiometric method, Renew. Sustain. Energy Rev. 74 (2017) 71–88. doi:10.1016/j.rser.2017.02.027.

[32] B. Reed, Kinetics of char gasification reactions above 500 ^{o}C, in: Encycl. Biomass Therm. Conversion, 3rd Ed, Biomass Energy Foundation Press, 2002: p. II-289.

[33] A.A. Ahmad, N.A. Zawawi, F.H. Kasim, A. Inayat, A. Khasri, Assessing the gasification performance of biomass: A review on biomass gasification process conditions, optimization and economic evaluation, Renew. Sustain. Energy Rev. 53 (2016) 1333–1347. doi:10.1016/j.rser.2015.09.030.

[34] J.A. Moulijn, M. Makkee, A.E. Van Diepen, Chemical process technology, 2nd ed., John Wiley & Sons Ltd., 2013.

[35] P. McKendry, Energy production from biomass (part 3): Gasification technologies, Bioresour. Technol. 83 (2002) 55–63. doi:10.1016/S0960-8524(01)00120-1.

[36] T.A. Milne, R.J. Evans, N. Abatzaglou, Biomass gasifier "'tars'": Their nature, formation, and conversion, Technical Report, 1998. doi:10.2172/3726.

[37] R. Warnecke, Gasification of biomass: Comparison of fixed bed and fluidized bed gasifier, Biomass and Bioenergy 18 (2000) 489–497. doi:10.1016/S0961-9534(00)00009-X.

[38] J.J. Hernández, M. Lapuerta, E. Monedero, Characterisation of residual char from biomass gasification: Effect of the gasifier operating conditions, J. Clean. Prod. 138 (2016) 83–93. doi:10.1016/j.jclepro.2016.05.120.

[39] J. Billaud, S. Valin, M. Peyrot, S. Salvador, Influence of steam, carbon dioxide and oxygen

addition on biomass gasification in entrained flow reactor conditions: Experiments and modelling, Fuel 166 (2016) 166–178. doi:10.1016/j.fuel.2015.10.046.

[40] K. Umeki, G. Häggström, A. Bach-Oller, K. Kirtania, E. Furusjö, Reduction of tar and soot formation from entrained-flow gasification of woody biomass by alkali impregnation, Energy and Fuels 31 (2017) 5104–5110. doi:10.1021/acs.energyfuels.6b03480.

[41] J.J. Hernández, G. Aranda, J. Barba, J.M. Mendoza, Effect of steam content in the air-steam flow on biomass entrained flow gasification, Fuel Process. Technol. 99 (2012) 43–55. doi:10.1016/j.fuproc.2012.01.030.

[42] J. Schneider, C. Grube, A. Herrmann, S. Rönsch, Atmospheric entrained-flow gasification of biomass and lignite for decentralized applications, Fuel Process. Technol. 152 (2016) 72–82. doi:10.1016/j.fuproc.2016.05.047.

[43] K. Qin, W. Lin, P.A. Jensen, A.D. Jensen, High-temperature entrained flow gasification of biomass, Fuel 93 (2012) 589–600. doi:10.1016/j.fuel.2011.10.063.

[44] Y. Zhang, S. Kajitani, M. Ashizawa, Y. Oki, Tar destruction and coke formation during rapid pyrolysis and gasification of biomass in a drop-tube furnace, Fuel 89 (2010) 302–309. doi:10.1016/j.fuel.2009.08.045.

[45] M. Rabaçal, S. Pereira, M. Costa, Review on pulverized combustion of non-woody residues, Energy & Fuels 32 (2017) 4069–4095. doi:10.1021/acs.energyfuels.7b03258.

[46] H. Yu, Z. Li, X. Yang, L. Jiang, Z. Zhang, D. Chen, Experimental research on oxygen-enriched gasification of straw in an entrained-flow gasifier, J. Renew. Sustain. Energy 5 (2013) 053127. doi:10.1063/1.4822260.

[47] M. Lapuerta, J.J. Hernández, A. Pazo, J. López, Gasification and co-gasification of biomass wastes: Effect of the biomass origin and the gasifier operating conditions, Fuel Process. Technol. 89 (2008) 828–837. doi:10.1016/j.fuproc.2008.02.001.

[48] J. Zhou, Q. Chen, H. Zhao, X. Cao, Q. Mei, Z. Luo, K. Cen, Biomass-oxygen gasification in a high-temperature entrained-flow gasifier, Biotechnol. Adv. 27 (2009) 606–611. doi:10.1016/j.biotechadv.2009.04.011.

[49] K. Qin, P.A. Jensen, W. Lin, A.D. Jensen, Biomass gasification behavior in an entrained flow reactor: Gas product distribution and soot formation, Energy and Fuels 26 (2012) 5992–6002. doi:10.1021/ef300960x.

[50] J.J. Hernández, G. Aranda-Almansa, A. Bula, Gasification of biomass wastes in an entrained flow gasifier: Effect of the particle size and the residence time, Fuel Process. Technol. 91 (2010) 681–692. doi:10.1016/j.fuproc.2010.01.018.

[51] B. Göktepe, K. Umeki, A. Hazim, T.S. Lundstrïum, R. Gebart, Soot reduction in an entrained flow gasifier of biomass by active dispersion of fuel particles, Fuel 201 (2017) 111–117. doi:10.1016/j.fuel.2016.09.039.

[52] B. Göktepe, K. Umeki, R. Gebart, Does distance among biomass particles affect soot formation in an entrained flow gasification process?, Fuel Process. Technol. 141 (2016). doi:10.1016/j.fuproc.2015.06.038.

[53] S. Septien, S. Valin, M. Peyrot, B. Spindler, S. Salvador, Influence of steam on gasification of millimetric wood particles in a drop tube reactor: Experiments and modelling, Fuel 103 (2013) 1080–1089. doi:10.1016/j.fuel.2012.09.011.

[54] A. V Bridgwater, The technical and economic feasibility of biomass gasif ication for power generation, Fuel 74 (1995) 631–653. doi:10.1016/0016-2361(95)00001-L.

[55] A. Van Der Drift, H. Boerrigter, B. Coda, M.K. Cieplik, K. Hemmes, R. Van Ree, H.J. Veringa, Entrained flow gasification of biomass: Ash behaviour, feeding issues, and system analyses, Energy research Centre of the Netherlands, 2004.

[56] J. Gil, J. Corella, M.P. Aznar, M.A. Caballero, Biomass gasification in atmospheric and bubbling fluidized bed: Effect of the type of gasifying agent on the product distribution, Biomass and Bioenergy 17 (1999) 389–403. doi:10.1016/S0961-9534(99)00055-0.

[57] G. Wang, R.B. Silva, J.L.T. Azevedo, S. Martins-Dias, M. Costa, Evaluation of the combustion behaviour and ash characteristics of biomass waste derived fuels, pine and coal in a drop tube furnace, Fuel 117 (2014) 809–824. doi:10.1016/j.fuel.2013.09.080.

[58] Dekati Low Pressure Impactor user manual ver. 3.4, (2007).

[59] L. Waldheim, T. Nilsson, Heating value of gases from biomass gasification, IEA Bioenergy Agreement, 2001.

[60] P.J. Woolcock, R.C. Brown, A review of cleaning technologies for biomass-derived syngas, Biomass and Bioenergy 52 (2013) 54–84. doi:10.1016/j.biombioe.2013.02.036.

[61] P.L. Spath, D.C. Dayton, Preliminary screening - Technical and economic assessment of synthesis gas to fuels and chemicals with emphasis on the potential for biomass-derived

syngas, Golden, CO, 2003. doi:10.2172/15006100.

VI. Appendix

VI.1 - Appendix A - In-House Made Cyclone

The char bin is composed by a bypass column (CB1), gas extracting column (CB2), solid sampling column (CB3) and a flow constraining cone (CB4). The technical drawing is shown in Figure VI-1.

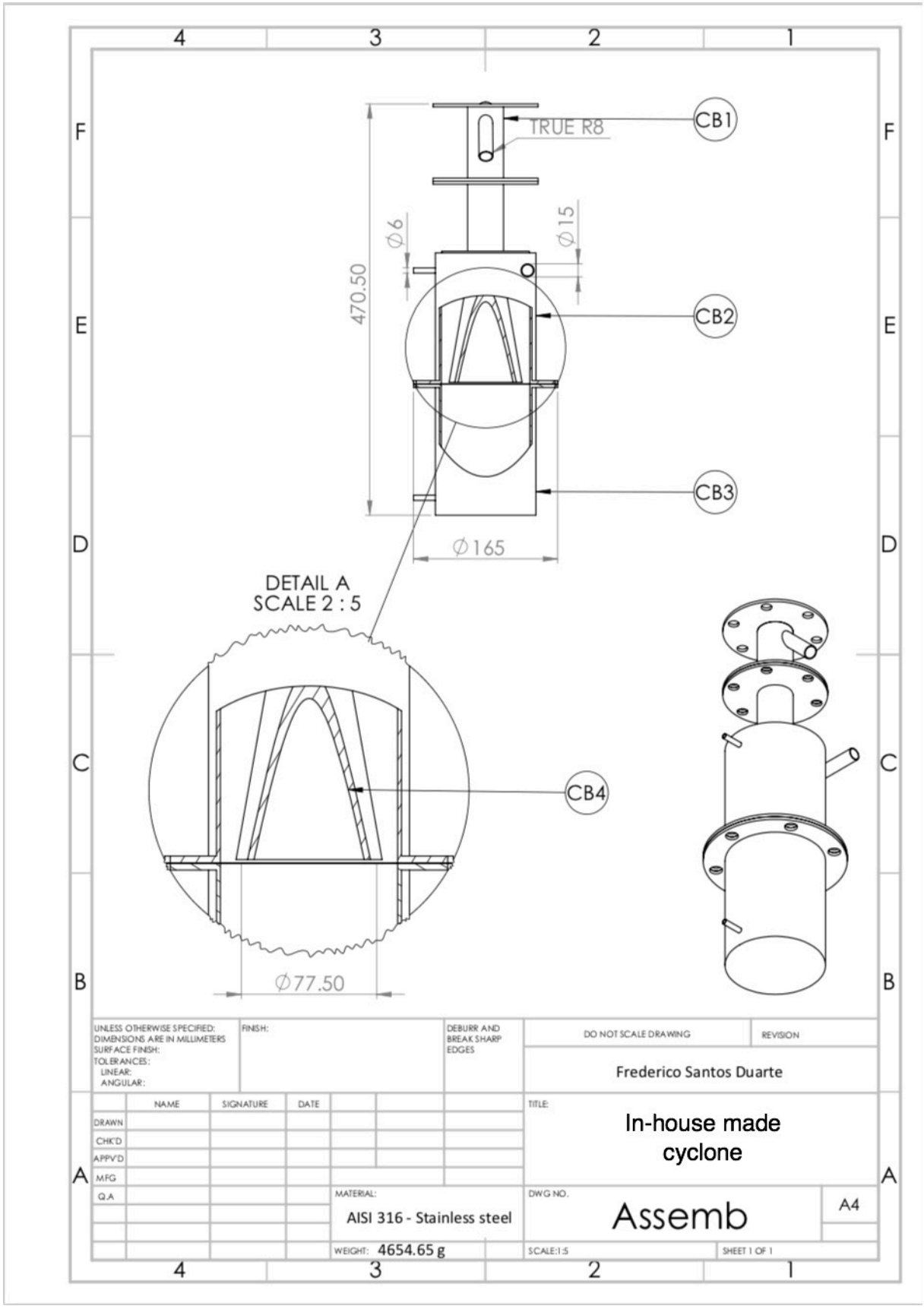

Figure VI-1– In- house made cyclone technical drawing.

VI.2 - Appendix B - Particulate Matter in the Impactor

Table VI-1 presents typical SEM images and EDS analysis results for the particulate matter collected in the thirteen-stages of the impactor at 1000 °C ($\lambda = 0.40$).

Table VI-1 - SEM images and EDS analysis for the particulate matter collected in the thirteen-stages of the impactor at 1000 °C ($\lambda = 0.4$).

Impactor Stage	SEM Image	EDS Analysis
13	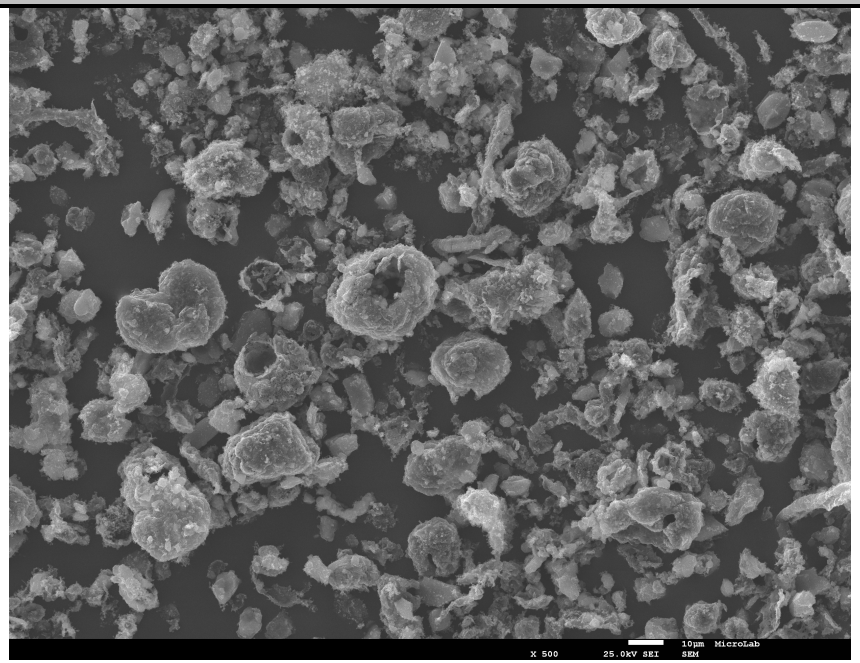	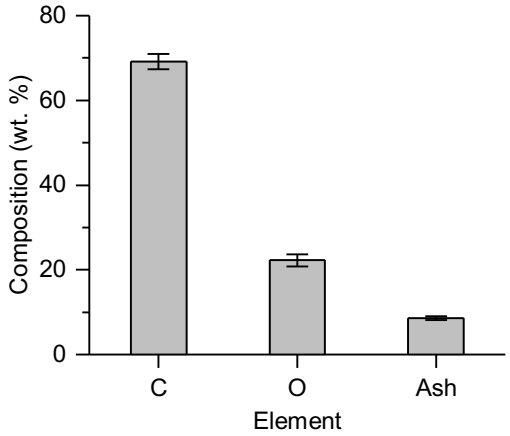

Impactor Stage	SEM Image	EDS Analysis
12	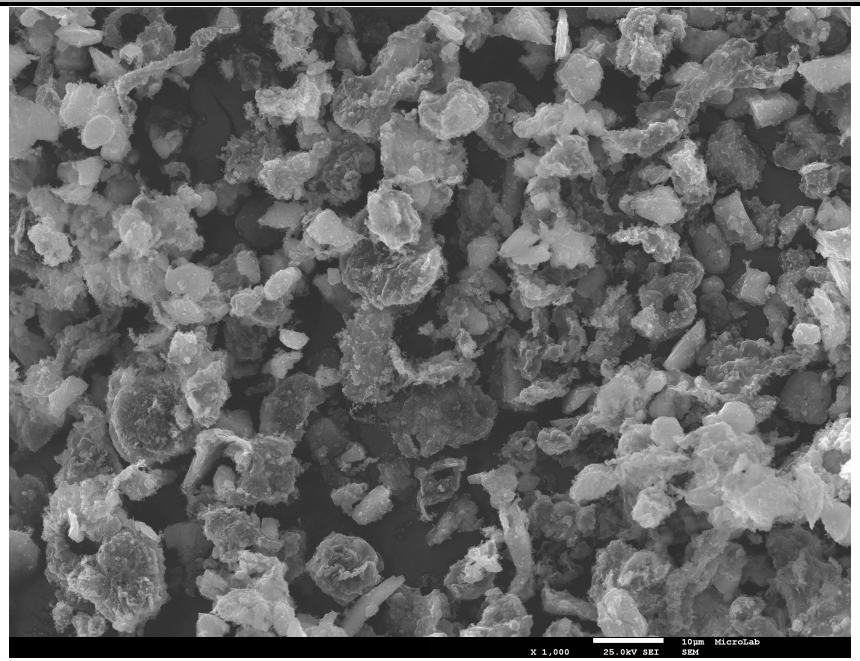	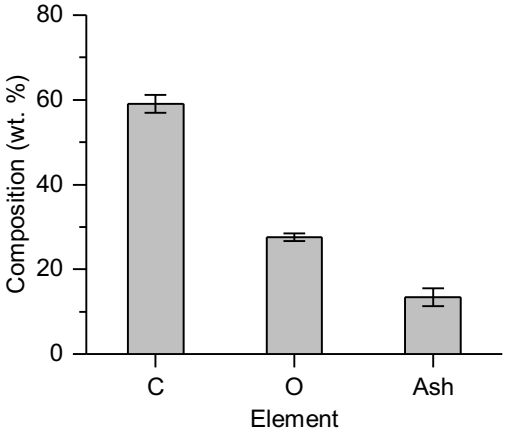

Impactor Stage	SEM Image	EDS Analysis
11	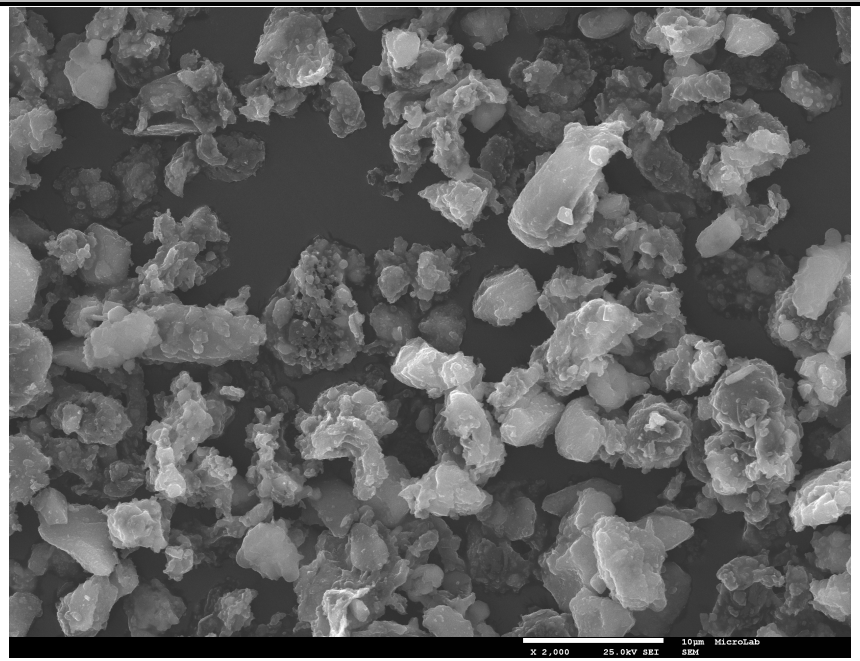	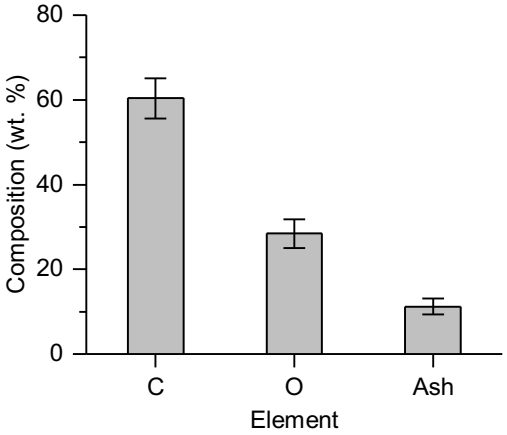

Impactor Stage	SEM Image	EDS Analysis
10	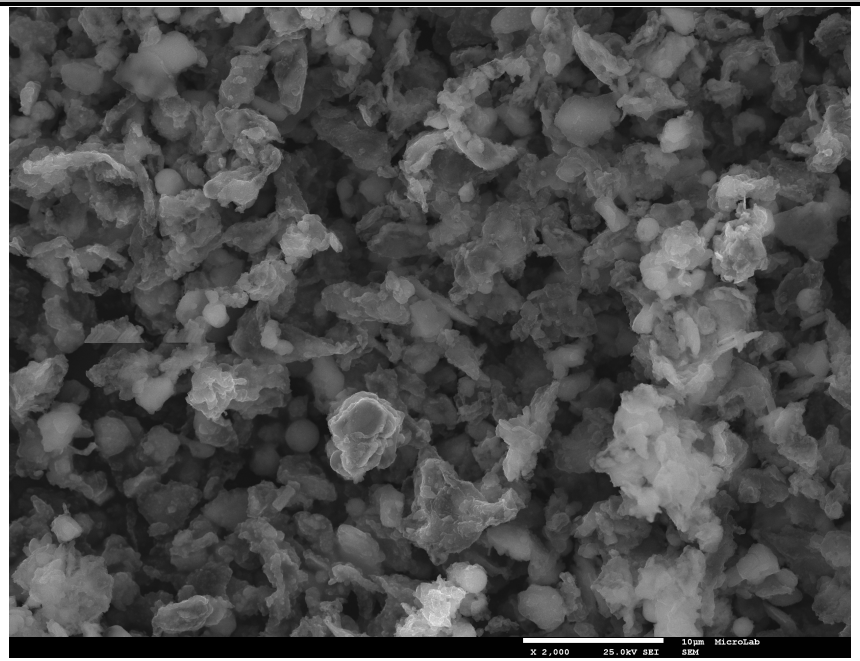	Not available

Impactor Stage	SEM Image	EDS Analysis
9	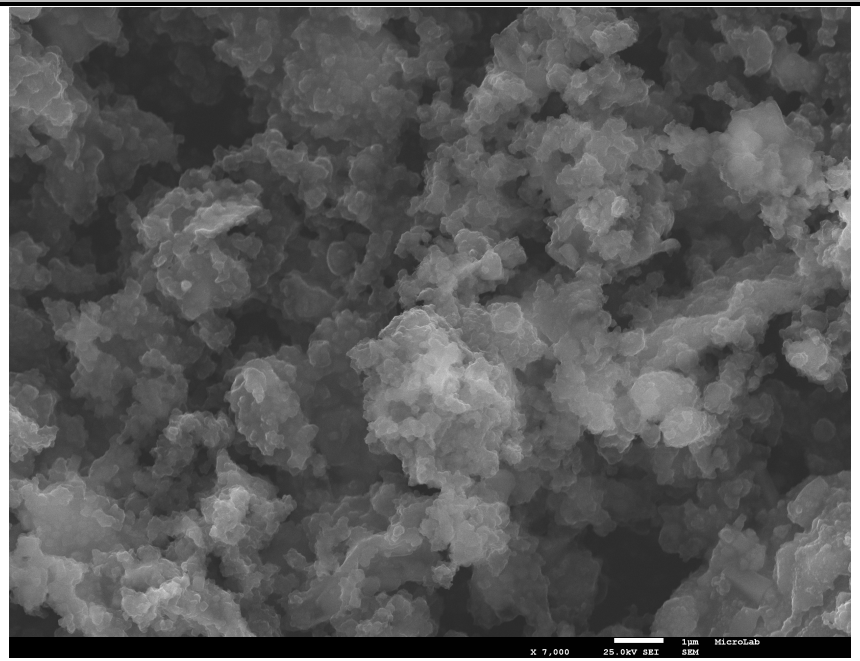	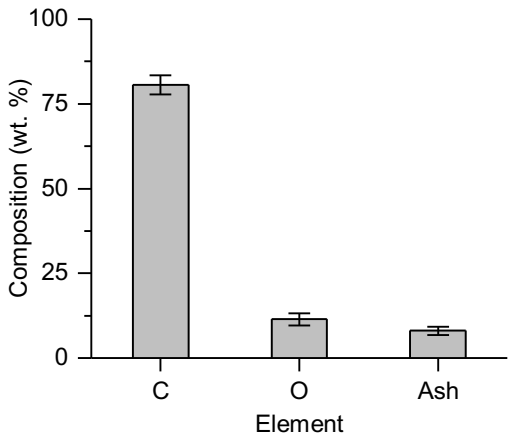

Impactor Stage	SEM Image	EDS Analysis
8	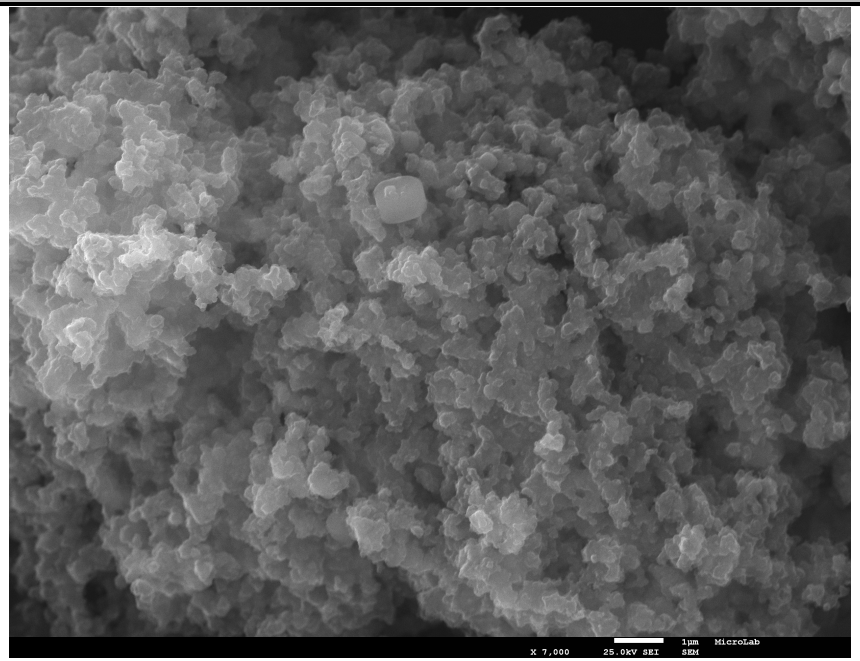	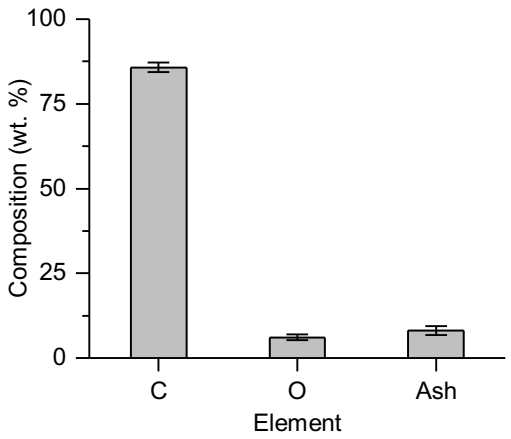

Impactor Stage	SEM Image	EDS Analysis
7	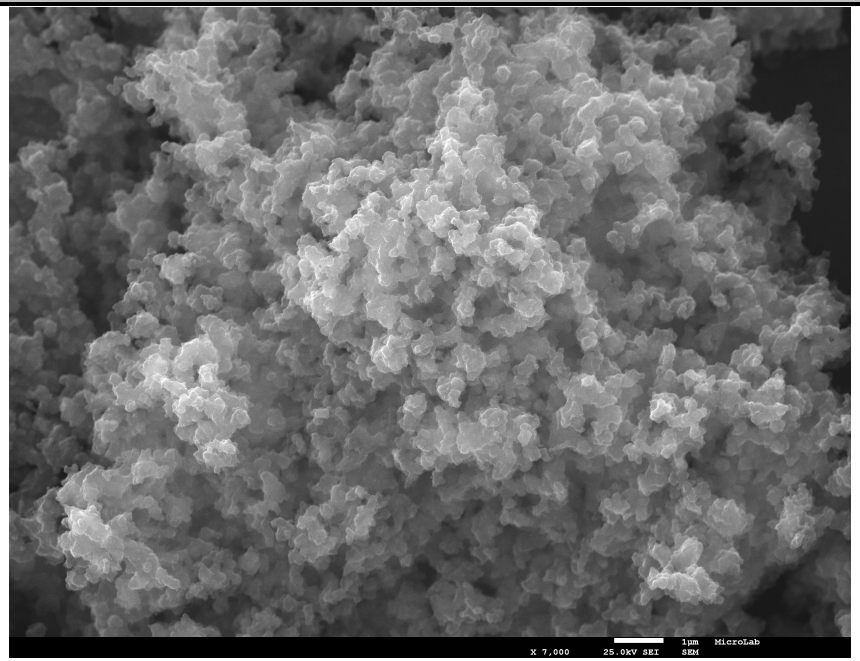	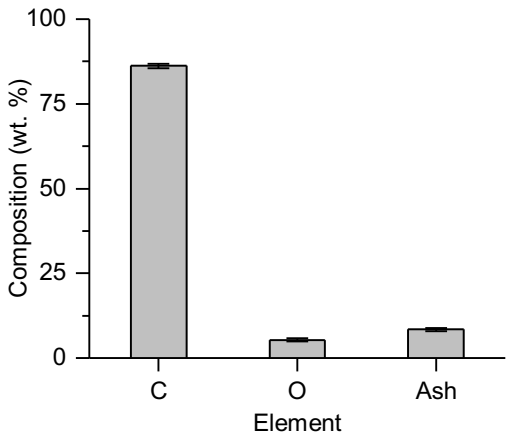

Impactor Stage	SEM Image	EDS Analysis
6	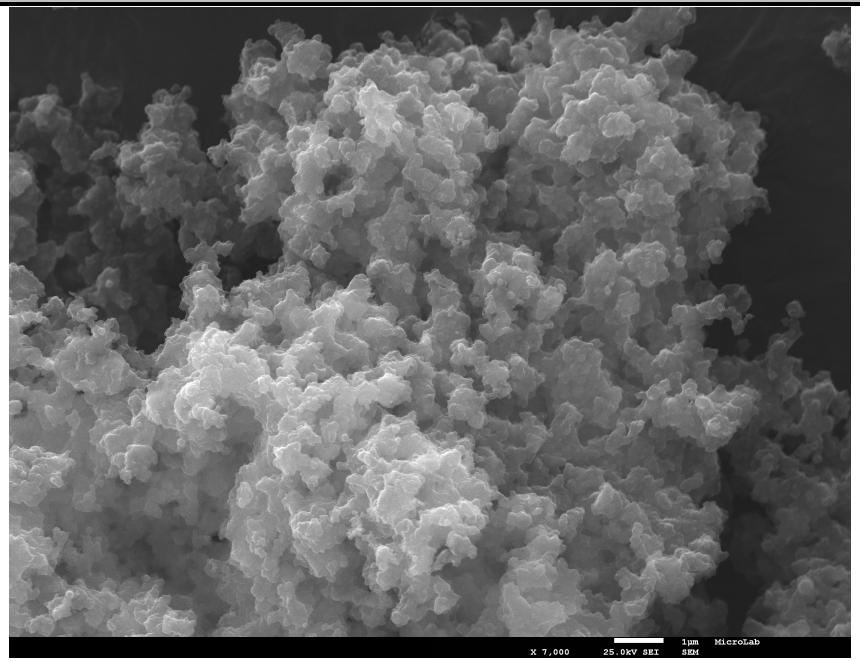	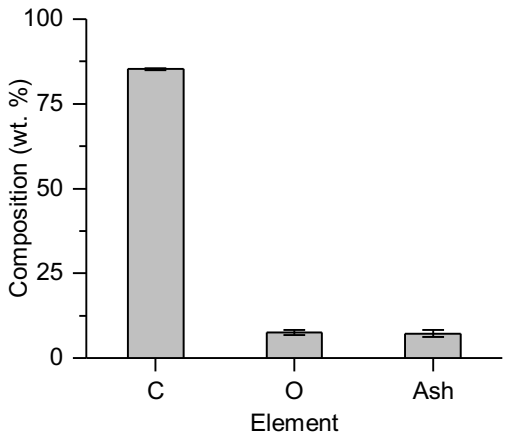

Impactor Stage	SEM Image	EDS Analysis
5	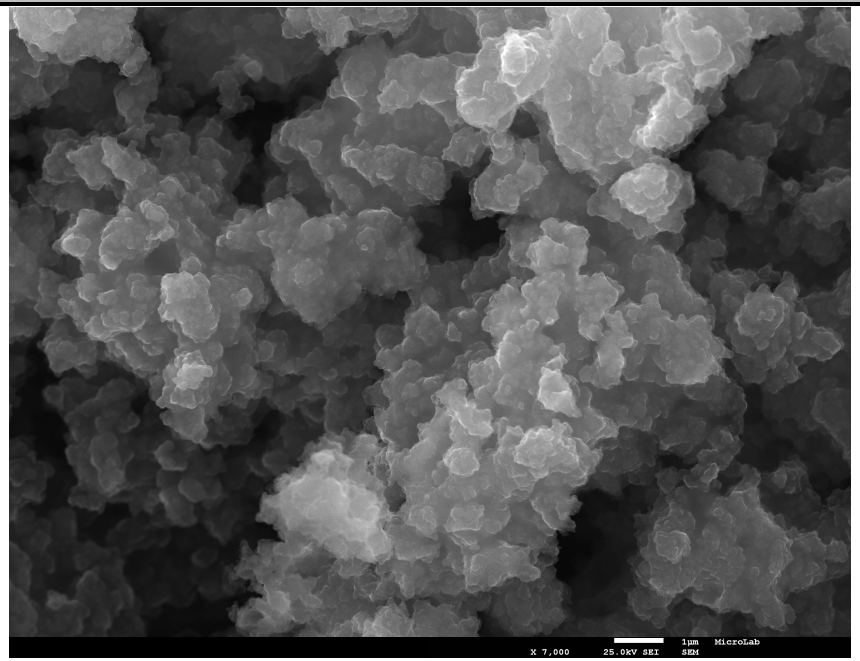	Not available

Impactor Stage	SEM Image	EDS Analysis
4	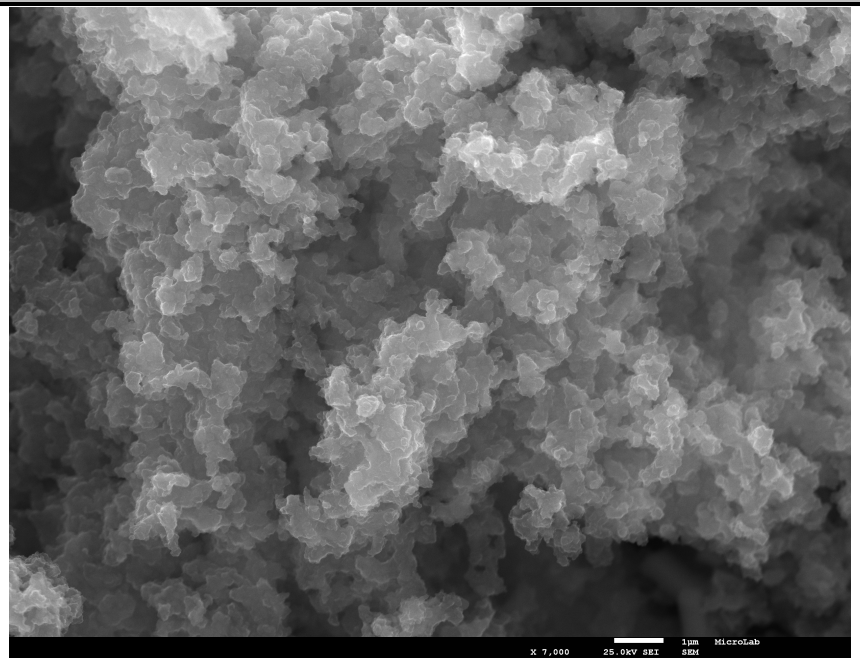	Not available

Impactor Stage	SEM Image	EDS Analysis
3	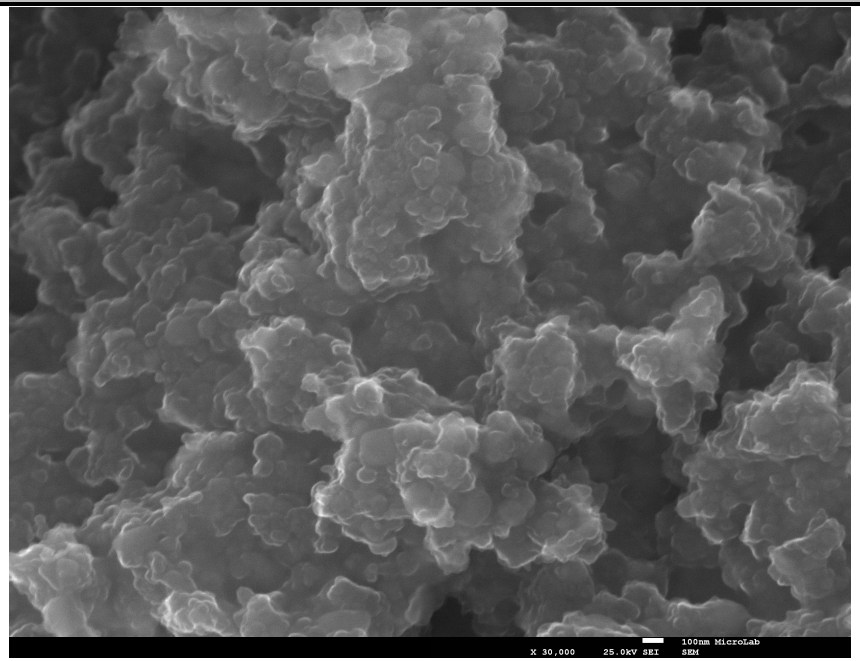	Not available

Impactor Stage	SEM Image	EDS Analysis
2	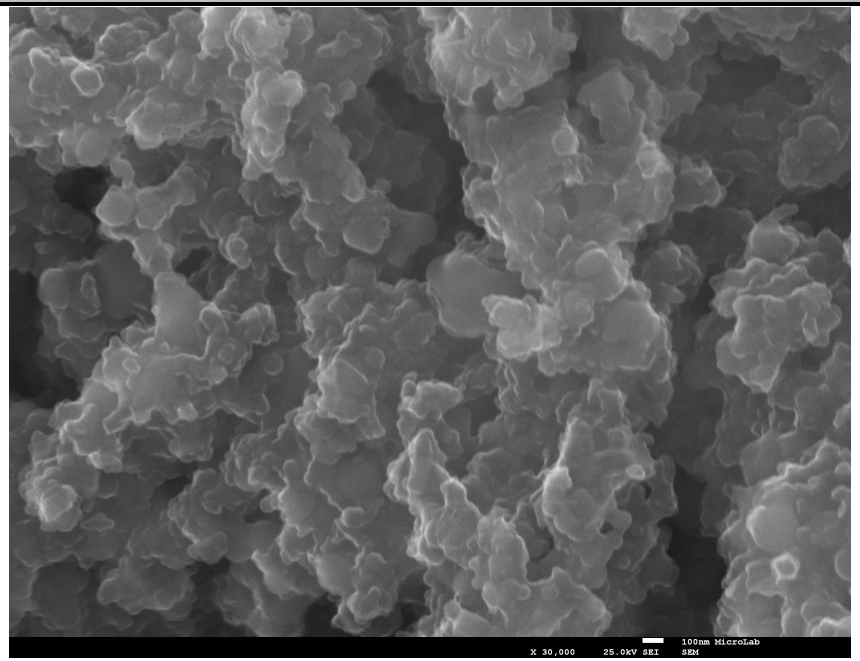	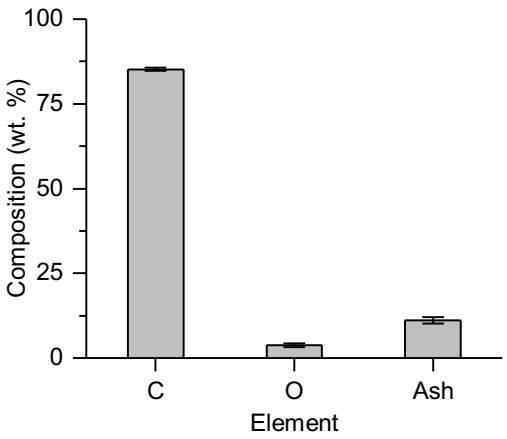

Impactor Stage	SEM Image	EDS Analysis
1